

# UCLA

## UCLA Previously Published Works

### Title

Bayesian modeling of interaction between features in sparse multivariate count data with application to microbiome study

### Permalink

<https://escholarship.org/uc/item/4qr9t31n>

### Journal

The Annals of Applied Statistics, 17(3)

### ISSN

1932-6157

### Authors

Zhang, Shuangjie

Shen, Yuning

Chen, Irene A

et al.

### Publication Date

2023

### DOI

10.1214/22-aos1690

### Copyright Information

This work is made available under the terms of a Creative Commons Attribution License, available at <https://creativecommons.org/licenses/by/4.0/>

Peer reviewed

# BAYESIAN MODELING OF INTERACTION BETWEEN FEATURES IN SPARSE MULTIVARIATE COUNT DATA WITH APPLICATION TO MICROBIOME STUDY

BY SHUANGJIE ZHANG<sup>1,\*</sup>, YUNING SHEN<sup>2</sup> IRENE A. CHEN<sup>2</sup> AND JUHEE LEE<sup>1</sup>

<sup>1</sup>*Department of Statistics, University of California Santa Cruz, \*szhan209@ucsc.edu; juheelee@soe.ucsc.edu*

<sup>2</sup>*Department of Chemical and Biomolecular Engineering, University of California Los Angeles, yshen@chem.ucsb.edu; ireneachen@ucla.edu*

Many statistical methods have been developed for the analysis of microbial community profiles, but due to the complexity of typical microbiome measurements, inference of interactions between microbial features remains challenging. We develop a Bayesian zero-inflated rounded log-normal kernel method to model interaction between microbial features in a community using multivariate count data in the presence of covariates and excess zeros. The model carefully constructs the interaction structure by imposing joint sparsity on the covariance matrix of the kernel and obtains a reliable estimate of the structure with a small sample size. The model also includes zero inflation to account for excess zeros observed in data and infers differential abundance of microbial features associated with covariates through log-linear regression. We provide simulation studies and real data analysis examples to demonstrate the developed model. Comparison of the model to a simpler model and popular alternatives in simulation studies shows that in addition to an added and important insight on the feature interaction, it yields superior parameter estimates and model fit in various settings.

**1. Introduction.** High-throughput sequencing (HTS) technologies in microbial ecology generate multivariate count data to characterize and analyze microbial communities from a variety of habitats such as human body sites, soil and water. Widely used sequencing methods in microbiome research include 16S ribosomal RNA (rRNA) sequencing and shotgun metagenomic sequencing (Jovel *et al.*, 2016). 16S rRNA gene sequencing utilizes PCR to target and amplify some portions of the bacterial 16S rRNA subunit gene for sequencing. The sequence reads are then clustered based on their similarity into operational taxonomic units (OTUs), which represent bacteria types. Following some initial preprocessing procedures, 16S rRNA sequencing data is summarized into a large count matrix (referred to as an OTU table) for downstream analyses, where the columns represent samples, and the rows contain multivariate count vectors of sequences corresponding to OTUs in the samples. Different from marker gene-based community profiling, shotgun metagenomic sequencing sequences a sample's entire metagenome and offers finer resolution at a higher cost. After some bioinformatic preprocessing, it also produces multivariate count table data that has structure and properties similar to those of an OTU table for downstream analyses. 16S rRNA sequencing datasets are used for illustrations of the statistical method developed in this work, but it can be considered for analysis of the data generated by either sequencing technique. We note that their analysis units are different, and the resulting statistical inferences may have different biological interpretations. In the human gut microbiome data, one of our real data examples in § 4.2, 16S rRNA sequencing data was collected to study how the composition of the gut microbiome is associated with inflammatory bowel disease (IBD) such as Crohn's disease

---

*Keywords and phrases:* Covariance Matrix, Differential Abundance, Factor Model, Joint Sparsity, Multivariate Count Data, Rounded Kernel Model, Zero Inflation.

(CD) or ulcerative colitis (UC) (Lloyd-Price *et al.*, 2019). Understanding how the composition of the human gut microbiome is associated with covariates such as disease status and age is important to provide insights on its role in human health and disease. Also, detecting and investigating the structure of microbial interactions is critical to better characterize microbial communities. Accurately accounting for the interactions can further improve the quantification of covariate effects on microbial abundances.

HTS sequencing data in microbiome study presents various challenges for statistical analysis due to high dimensionality and some added complexity. Total OTU counts vary in samples due to experimental artifacts such as the sequencing depth, and raw counts do not reflect actual microbial abundances (called compositionality). Consequently, normalization of OTU counts is needed for meaningful comparison across samples. In addition, the high-dimensional structure with excess zeros and over-dispersion further complicates the analysis of an OTU table and calls for flexible statistical models. While various statistical models have been proposed for microbiome data analysis, most existing methods focus on either inference on the effects of environmental factors (i.e., covariate) on microbial abundances or their absence/presence or inference on associations between microbes. For studying associations with covariates, generalized regression models are popular. For example, Poisson or negative binomial (NB) regression models are one of the common approaches, where covariates are related to expected counts through a log-linear regression framework. Those models include sample size factors for normalization. Zero-inflated (ZI) Poisson or ZI-NB models are also utilized to address excess zeros. Under a ZI model, a count is distributed as a mixture, a component of which is the distribution with a point mass of one at zero. See Li *et al.* (2017), Zhang *et al.* (2017), Jiang *et al.* (2021), Shuler *et al.* (2021) among many others, for examples of using Poisson or NB regression models. Another common regression approach uses multinomial or ZI multinomial models, where a similar log-linear regression framework is used to relate covariates to (unconstrained) occurrence probability vectors, e.g., Xia *et al.* (2013), Wadsworth *et al.* (2017), Ren *et al.* (2017), Tang and Chen (2019) and Grantham *et al.* (2020) among many others. In particular, Grantham *et al.* (2020) proposed a Bayesian multinomial regression model that assumes a mixed effects model for unconstrained occurrence probabilities and uses a latent factor model for the covariance matrix of the prior distribution of the unconstrained probabilities. However, the implication of the covariance among unconstrained probabilities for microbial interactions is not clear due to the fixed total count constraint under the assumed multinomial distribution. Approaches of using a Dirichlet-tree multinomial model were also proposed to exploit the tree structure information via a phylogenetic tree, e.g., Wang and Zhao (2017), Mao, Chen and Ma (2020) and Wang, Mao and Ma (2021). They assume potential associations between microbes that have similar sequences but do not attempt to infer microbial interactions. Alternatively, Paulson *et al.* (2013) assumed a univariate log-normal distribution for individual counts after adding a pseudo count to observed counts and used regression to relate covariates to OTU abundances. For inferences on microbial interactions, correlations between pairs of microbes based on some transformed OTU counts are commonly used as a measure. The task of estimating correlations between microbes is complicated due to the aforementioned challenges. Centered-log-ratio (clr) transformation is usually applied to raw counts prior to analysis for compositionality, and small pseudo-counts are added to avoid numerical issues of excess zeros. To address high dimensionality, an additional structure such as sparsity through  $\ell_1$  penalty is often imposed on the covariance matrix or precision matrix for reliable inference. For example, SparCC in Friedman and Alm (2012) normalizes raw counts by sample total counts after adding pseudo counts and models log-transformed ratios of the normalized counts to infer correlations between OTUs. CCLasso in Fang *et al.* (2015) models log-transformed counts and provides a least

squares estimate of a correlation matrix with  $\ell_1$  penalty under some constraint for compositionality of microbiome data. SPIEC-EASI in Kurtz *et al.* (2015) builds an undirected graphical model for clr transformed data and yields inference on an association network between OTUs through a precision matrix. Sparsity is assumed for the underlying association network. Schwager *et al.* (2017) uses a Bayesian log-normal graphical model for unconstrained counts. A LASSO prior is used for the precision matrix. Similarly, Prost, Gazut and Bruls (2021) developed a likelihood-based zero-inflated log-normal graphical model (Zi-LN) that appropriately accounts for excess zeros in microbiome data. Graphical LASSO (Friedman, Hastie and Tibshirani, 2008) is used for estimation of the precision matrix. While existing methods can provide useful insights on microbial communities, methods that jointly infer associations between microbes and their associations with covariates are still lacking. Furthermore, statistical methods that carefully address excess zeros, compositionality and high dimensionality are needed for accurate inference on the associations.

To obtain a better understanding of the underlying biological processes, we develop a Bayesian rounded kernel regression model with zero inflation. The model enables a direct assessment of interrelationships between OTUs and their associations with covariates. The developed method directly models raw counts and simultaneously performs model-based normalization through random sample scale factors for compositionality. Specifically, we use a multivariate log-normal distribution as the kernel and define multivariate count responses  $\mathbf{Y} = (Y_1, \dots, Y_J)$  of  $J$  OTUs in terms of multivariate log-normal latent variables  $\mathbf{Y}^* = (Y_1^*, \dots, Y_J^*)$  using fixed thresholds. We then relate covariates  $\mathbf{x}$  to the mean vector  $\boldsymbol{\mu}$  of the distribution of  $\mathbf{Y}^*$  through regression and use the covariance matrix  $\Sigma$  to characterize interrelationship among OTUs.  $\boldsymbol{\mu}$  also includes sample size factors for normalization. For  $\Sigma$ , we assume joint sparsity to reliably learn a high dimensional covariance structure with a small sample size. Sparsity assumption is commonly used in the covariance matrix estimation when  $p \gg n$  (e.g., Cai, Ren and Zhou (2016), Pati *et al.* (2014), Gao and Zhou (2015), Xie *et al.* (2018)). Specifically, we develop a joint sparse latent factor model for  $\Sigma$ , where we let the number of factors much smaller than the number of OTUs (features), and a majority of OTUs can have factor loadings close to zero, i.e., feature selection. The model greatly reduces the number of parameters to estimate and provides a simple interpretation of the interrelationship structure. The representation of the model with independent latent factors also allows introducing zero inflation in a convenient manner. The model appropriately accounts for excess zeros due to the absence of an OTU or the undersampling of a rare OTU, and  $\Sigma$  provides inferences on the interrelationship structure among OTUs present in a sample. In addition, overdispersion is accommodated through random effects, resulting in further improvement in the inference.

In the remainder of the paper, we describe the model and its applications. § 2 describes the zero-inflated multivariate log-normal kernel model (called “ZI-MLN”), and § 3 has results of simulation studies to evaluate the performance of our method. § 4 has results from the model applied to two real datasets, and § 5 concludes with some discussion of the results and areas of future research.

## 2. Statistical Model.

*2.1. Sampling Distribution and Prior Specification.* Consider multivariate count data obtained for  $J$  OTUs in a microbiome study. We let  $\mathbf{Y}_i = (Y_{i1}, \dots, Y_{iJ})$  denote a  $J$ -dimensional random count vector of OTU counts of sample  $i = 1, \dots, N$  taken from subject  $g_i \in \{1, \dots, M\}$ , where  $Y_{ij} \in \mathbb{N}^0$  is the count of OTU  $j = 1, \dots, J$  in sample  $i$ . We let  $n_m$  be the number of samples taken from subject  $m$  and have  $N = \sum_{m=1}^M n_m$ . In addition, data may include a set of  $P$  covariates,  $\mathbf{x}_i = (x_{i1}, \dots, x_{iP})$ . Our skin microbiome dataset in

§ 4.1 consists of observed counts of 187 OTUs in 20 samples, one sample from each of 20 subjects. The dataset does not have covariates besides the subject factor. Human gut microbiome data in § 4.2 includes 67 samples collected from multiple biopsy sites of 37 patients. 107 OTUs are included with covariates such as disease phenotype and age for analysis. The model simultaneously infers the interaction structure of OTUs and the differential abundance of OTUs by covariates. It can also be easily simplified if no covariate is available, as we will show later.

We consider a Bayesian rounded multivariate log-normal kernel model for  $\mathbf{Y}_i$  in [Canale and Dunson \(2011\)](#). We first introduce continuous latent variables  $\mathbf{Y}_i^* = (Y_{i1}^*, \dots, Y_{iJ}^*)$  with  $Y_{ij}^* \in \mathbb{R}^+$ ,  $i = 1, \dots, n$  and  $j = 1, \dots, J$ , and assume

$$(1) \quad \mathbf{Y}_i^* \mid \boldsymbol{\mu}_i, \Sigma \stackrel{\text{indep}}{\sim} \log\text{-N}_J(\boldsymbol{\mu}_i, \Sigma),$$

where parameters  $\boldsymbol{\mu}_i = (\mu_{i1}, \dots, \mu_{iJ})' \in \mathbb{R}^J$  and  $\Sigma > 0$ . In (1), we have the mean  $E(Y_{ij}^* \mid \boldsymbol{\mu}_i, \Sigma) = \exp(\mu_{ij} + \frac{1}{2}\Sigma_{jj})$ , the median  $Q_{0.5} = \exp(\mu_{ij})$  and covariance  $\text{Cov}(Y_{ij}^*, Y_{ij'}^*) = \exp\{\mu_{ij} + \mu_{ij'} + \frac{1}{2}(\Sigma_{jj} + \Sigma_{j'j'})\} \{\exp(\Sigma_{jj'}) - 1\} = E(Y_{ij}^*)E(Y_{ij'}^*)\{\exp(\Sigma_{jj'}) - 1\}$ . We next use a threshold function to relate  $Y_{ij}^*$  to  $Y_{ij}$  by letting  $Y_{ij} = y_j$  if  $y_j \leq Y_{ij}^* < (y_j + 1)$ . The multivariate log-normal density is zero for a vector with negative values, and the kernel defines a valid multivariate distribution for  $\mathbf{Y}$ . We further let  $\tilde{\mathbf{Y}}_i^* = (\tilde{Y}_{i1}^*, \dots, \tilde{Y}_{iJ}^*)$  with  $\tilde{Y}_{ij}^* = \log(Y_{ij}^*) \in \mathbb{R}$  and have

$$(2) \quad \begin{aligned} \mathbb{P}(\mathbf{Y}_i = \mathbf{y}_i \mid \boldsymbol{\mu}_i, \Sigma) &= \int_{A(\mathbf{y}_i)} f_{\mathbf{y}^*}(\mathbf{y}^* \mid \boldsymbol{\mu}_i, \Sigma) d\mathbf{y}^* \\ &= \int_{\tilde{A}(\mathbf{y}_i)} \phi_J(\tilde{\mathbf{y}}^* \mid \boldsymbol{\mu}_i, \Sigma) d\tilde{\mathbf{y}}^*, \end{aligned}$$

where  $f_{\mathbf{y}^*}$  represents the density function of the  $J$ -dimensional log-normal distribution with parameters  $\boldsymbol{\mu}_i$  and  $\Sigma$ , and  $\phi_J$  the density function of a  $J$ -dimensional normal distribution. The regions of integration are  $A(\mathbf{y}_i) = \{\mathbf{y}^* \mid y_{i1} \leq y_1^* < y_{i1} + 1, \dots, y_{iJ} \leq y_J^* < y_{iJ} + 1\}$  and  $\tilde{A}(\mathbf{y}_i) = \{\tilde{\mathbf{y}}^* \mid \log(y_{i1}) \leq \tilde{y}_1^* < \log(y_{i1} + 1), \dots, \log(y_{iJ}) \leq \tilde{y}_J^* < \log(y_{iJ} + 1)\}$ . The properties of the distribution of  $Y_{ij}^*$ 's such as their means and covariances can be easily computed from (2). For example, we find  $E(Y_{ij} \mid \mu_{ij}, \Sigma_{jj}) = \sum_{b=0}^{\infty} b \mathbb{P}(Y_{ij} = b \mid \mu_{ij}, \Sigma_{jj})$  with  $\mathbb{P}(Y_{ij} = b \mid \mu_{ij}, \Sigma_{jj}) = \Phi_1(\log(b+1) \mid \mu_{ij}, \Sigma_{jj}) - \Phi_1(\log(b) \mid \mu_{ij}, \Sigma_{jj})$ , where  $\Phi_d(\cdot \mid a, \mathbf{B})$  is the cdf of the  $d$ -variate normal distribution with mean  $a$  and (co)variance  $\mathbf{B}$ . A large value of  $\mu_{ij}$  thus implies high abundance of OTU  $j$  in sample  $i$ . We express  $\mu_i$  as a function of covariates, sample-size factor and OTU-size factor. The factors account for differences in sample total counts and variability in baseline OTU abundances. We will give a regression model for  $\boldsymbol{\mu}_i$  below. We can also compute variances and covariances of the counts. In particular,  $\text{Cov}(Y_{ij}, Y_{ij'} \mid \boldsymbol{\mu}_i, \Sigma) = \sum_{b=0}^{\infty} \sum_{b'=0}^{\infty} bb' \mathbb{P}(Y_{ij} = b, Y_{ij'} = b' \mid \boldsymbol{\mu}_i, \Sigma) - E(Y_{ij} \mid \mu_{ij}, \Sigma_{jj})E(Y_{ij'} \mid \mu_{ij'}, \Sigma_{j'j'})$ .  $\mathbb{P}(Y_{ij} = b, Y_{ij'} = b' \mid \boldsymbol{\mu}_i, \Sigma)$  can be computed with a bivariate normal distribution in a way similar to  $\mathbb{P}(Y_{ij} = b \mid \mu_{ij}, \Sigma_{jj})$ . Under (2), the counts of OTUs  $j$  and  $j'$  are dependent if  $\Sigma_{jj'} \neq 0$ . That is,  $\Sigma$  characterizes microbial interactions with a straightforward interpretation. In addition, overdispersion is known to be common in sequencing data and can be properly accommodated through heavy tails of a log-normal distribution.

We next build a prior distribution for  $\Sigma$ . The number of OTUs  $J$  is often much greater than the sample size  $N$  in microbiome studies, i.e.,  $J \gg N$ . In a high-dimensional setting, the sample covariance matrix is singular and provides an unstable estimate for  $\Sigma$ . To overcome the difficulty, it is common that structural assumptions are imposed on  $\Sigma$  ([Cai, Ren and Zhou, 2016](#)). For example, [Friedman, Hastie and Tibshirani \(2008\)](#), [Bien and Tibshirani](#)

(2011) and Cai, Liu and Luo (2011) consider the sparsity assumption that most of the elements in  $\Sigma$  (or  $\Sigma^{-1}$ ) are zero or negligible for marginal independencies between features (or conditional independencies). In particular,  $\ell_1$  penalty is used to shrink the elements of  $\Sigma$  (or  $\Sigma^{-1}$ ) to zero. Alternatively, a low-rank structure is considered, sometimes jointly with the sparsity assumption (called joint sparsity). For example, see Cai, Ma and Wu (2015); Bhattacharya *et al.* (2015) and Xie *et al.* (2018). The joint sparsity structure allows to achieve good theoretical properties, such as faster minimax rate of convergence and tighter posterior contraction rate for estimating a covariance matrix (Cai, Ma and Wu, 2015; Xie *et al.*, 2018). Taking the latter approach, we first decompose  $\Sigma$  as

$$(3) \quad \Sigma = \Lambda\Lambda' + \sigma^2\mathbf{I}_J,$$

where  $\lambda_j = [\lambda_{j1}, \dots, \lambda_{jk}]'$  and  $\Lambda = [\lambda_1', \dots, \lambda_J']'$  is a  $J \times K$  factor loading matrix with  $K \ll J$ . The model assumes most of the covariance structure between OTUs is explained by a small number of factors to obtain a more accurate and reliable estimate of  $\Sigma$  in the case of  $N \ll J$ . We assume an isotropic noise and consider a conditionally conjugate prior distribution  $\sigma^2 \sim \text{inv-Ga}(a_\sigma, b_\sigma)$  with fixed  $a_\sigma$  and  $b_\sigma$  for easy computation. If needed, independent idiosyncratic noise can be considered by letting  $\Sigma = \Lambda\Lambda' + \text{diag}(\sigma_j^2)$  and  $\sigma_j^2 \stackrel{iid}{\sim} \text{inv-Ga}(a_\sigma, b_\sigma)$ . We introduce joint sparsity on  $\Sigma$  by considering a Dirichlet-Laplace prior in Bhattacharya *et al.* (2015),

$$(4) \quad \begin{aligned} \tau_k &| a_\tau, b_\tau \stackrel{iid}{\sim} \text{Ga}(a_\tau, b_\tau), \\ \phi &= (\phi_1, \dots, \phi_J) | a_\phi \sim \text{Dir}(a_\phi, \dots, a_\phi), \\ \lambda_{jk} &| \phi_j, \tau_k \stackrel{indep}{\sim} \text{DE}(\phi_j \tau_k), \end{aligned}$$

where  $\text{DE}(a)$  represents the double-exponential (Laplace) distribution with scale parameter  $a$ , and  $\text{Ga}(a, b)$  is the gamma distribution with shape parameter  $a$  and scale parameter  $b$  (so mean  $a/b$ ). Under the model in (4), a small value of  $\phi_j$  shrinks  $\lambda_{jk}$  toward zero for all  $k$ , and  $\Sigma_{jj'}$  tends to have small values for all  $j'$ . That is,  $\phi_j$  induces joint sparsity for  $\Sigma$  together with  $K$ . OTUs with a small value of  $\phi_j$  may be those less interacting with other OTUs. The model provides an easy interpretation of the interrelationships between OTUs and reliable inference even for cases with  $N \ll J$ . The double-exponential distribution for  $\lambda_{jk}$  has heavier tails and a more pointed center than the normal distribution that is a convenient choice, and facilitates sparsity in  $\lambda_{jk}$ , resulting in sparsity in  $\Sigma$ . Theorem 3.1 of Bhattacharya *et al.* (2015) proves that when  $a_\phi$  is set to be  $J^{-(1+b)}$  for any  $b > 0$ , the posterior contraction rate of  $\lambda_{jk}$  achieves the minimax rate. However, our simulation studies show that the model with  $a_\phi = 1/J$  tends to overshrink  $\lambda_{jk}$  even when only a small number of OTUs interact, and we fix  $a_\phi = 1/2$  with soften conditions for the contraction rate. We fix the factor dimension  $K$  at a reasonably large value for computational convenience. If desired, an exponentially decaying prior such as a Poisson distribution can be placed on  $K$  to attain optimal posterior contraction rate (Pati *et al.*, 2014). Pati *et al.* (2014) used the Dirichlet-Laplace prior for vectorized loadings  $\text{vec}(\Lambda)$  in a Bayesian factor model for a multivariate normal outcome vector with mean zero and did not attempt to induce a joint sparsity structure. Xie *et al.* (2018) used a spike-and-slab prior for  $\phi_j$  and developed a matrix spike-and-slab LASSO prior under the Gaussian sampling distribution assumption. However, placing spike-and-slab priors for individual matrix elements may cause computational difficulties, especially for large  $J$ . Similar to Bhattacharya and Dunson (2011) and Xie *et al.* (2018), we do not place any constraints on  $\Lambda$  such as orthogonality of the columns nor attempt to interpret latent factors since the primary interest of inference is on  $\Sigma$ .



We re-write the model in (1) and (3) by introducing a latent normal vector  $\boldsymbol{\eta}_i \stackrel{iid}{\sim} \mathbf{N}_K(0, \mathbf{I}_K)$ ;

$$(5) \quad \tilde{Y}_{ij}^* \mid \mu_{ij}, \boldsymbol{\lambda}_j, \boldsymbol{\eta}_i, \sigma^2 \stackrel{indep}{\sim} \mathbf{N}_1(\mu_{ij} + \boldsymbol{\lambda}'_j \boldsymbol{\eta}_i, \sigma^2).$$

By integrating over  $\boldsymbol{\eta}_i$ , we obtain the normal distribution with covariance matrix  $\Sigma$  in (3) for  $\tilde{Y}_{ij}^*$ . The conditional independence between  $\tilde{Y}_{ij}^*$  given  $\boldsymbol{\eta}_i$  in (5) greatly facilitates the posterior computation. Furthermore, it enables easy implementation of a zero-inflated model. Excess zeros in microbiome data are very common. If excess zeros are not compatible with the distribution in (2), the resulting inferences can be distorted. For a zero-inflated model, we introduce binary indicators  $\delta_{ij}$  that represent the absence/presence of OTUs, and assume  $\delta_{ij} \mid \epsilon_{ij} \stackrel{indep}{\sim} \text{Ber}(\epsilon_{ij})$ , where  $\epsilon_{ij}$  is the probability of OTU  $j$  being absent in sample  $i$ . We let  $\delta_{ij} = 1$  indicate the absence of OTU  $j$  in sample  $i$ , so  $Y_{ij} = 0$ . Given  $\delta_{ij} = 0$ , we assume, for  $y = 0, 1, 2, \dots$ ,

$$(6) \quad \begin{aligned} \mathbb{P}(Y_{ij} = y \mid \mu_{ij}, \boldsymbol{\lambda}_j, \boldsymbol{\eta}_i, \sigma^2, \delta_{ij} = 0) = & \Phi_1(\log(y+1) \mid \mu_{ij} + \boldsymbol{\lambda}'_j \boldsymbol{\eta}_i, \sigma^2) \\ & - \Phi_1(\log(y) \mid \mu_{ij} + \boldsymbol{\lambda}'_j \boldsymbol{\eta}_i, \sigma^2). \end{aligned}$$

Given the presence of an OTU, the model in (6) generates counts, some of which can be zero. Given  $\boldsymbol{\delta}_i = (\delta_{i1}, \dots, \delta_{iJ})$ , a vector of  $\tilde{Y}_{ij}^*$  with  $\delta_{ij} = 0$  follows a multivariate normal distribution, and its mean vector and covariance matrix are a subvector of  $\boldsymbol{\mu}_i$  omitting the elements with  $\delta_{ij} = 1$  and a submatrix of  $\Sigma$  omitting the rows and columns with  $\delta_{ij} = 1$ , respectively. That is,  $\boldsymbol{\mu}_i$  and  $\Sigma$  provide inferences on the mean abundance and interrelationship structure even when the zero inflation component is added to the model. We relate covariates  $\mathbf{x}_i$  to the probability of  $\delta_{ij} = 1$  by using a probit link function,

$$(7) \quad \epsilon_{ij} = \Phi_1(\kappa_{j0} + \mathbf{x}'_i \boldsymbol{\kappa}_j \mid 0, 1),$$

where  $\kappa_{j0}$  and  $\boldsymbol{\kappa}_j = (\kappa_{j1}, \dots, \kappa_{jP})'$  are parameters that quantify the effects of  $\mathbf{x}_i$  on  $\epsilon_{ij}$ . We consider a normal distribution for the prior of  $\kappa_{jp}$ ,  $\kappa_{jp} \stackrel{iid}{\sim} \mathbf{N}(\bar{\kappa}_p, u_{\kappa}^2)$ ,  $p = 0, \dots, P$ . With a high proportion of zero counts, adding subject specific random effects into  $\epsilon_{ij}$  may produce unstable model fitting (Agarwal, Gelfand and Citron-Pousty, 2002). Thus, the model in (7) does not include subject specific random effects.

Lastly, we relate covariates  $\mathbf{x}_i$  and subject-specific group factors  $g_i$  to the mean OTU abundances through  $\mu_{ij}$ ;

$$(8) \quad \mu_{ij} = r_i + \alpha_j + \mathbf{x}'_i \boldsymbol{\beta}_j + s_{g_i, j}.$$

$r_i$  and  $\alpha_j$  are sample size factors and OTU size factors, respectively. The observed OTU counts are a product of both the library size (total number of reads) and the OTU baseline abundance.  $r_i$ 's normalize OTU counts across samples, and  $\alpha_j$ 's account for variability in OTU baseline abundances. We let  $r_i$  and  $\alpha_j$  random. Thus, the model performs model-based normalization and addresses compositionality. We will specify priors of  $r_i$  and  $\alpha_j$  below. In (8), regression coefficients  $\beta_{jp}$  quantify the change in the abundance of OTU  $j$  from the mean abundance by  $x_{ip}$  (so-called a factor effects model in an ANOVA setting). Under the formulation, choosing a reference category for a categorical covariate is not required, and an implicit assumption of the presence of an OTU under the arbitrarily chosen reference category is not needed to infer the effects of the other categories. When any covariate is categorical,  $\mathbf{x}_i$  in (8) is different from that in (7) due to a different parameterization of the covariate. An example will be illustrated in § 3.2. When no covariate is available as in Simulation 1 in § 3.1 and the skin microbiome data in § 4.1, we simply drop the regression terms  $\mathbf{x}'_i \boldsymbol{\kappa}_j$  and  $\mathbf{x}'_i \boldsymbol{\beta}_j$  from (7) and (8), respectively, and use the simplified model to infer OTU interaction

structure.  $s_{g_i,j}$ 's in (8) are random effects to account for between-subject heterogeneity and induce dependence among the samples collected from the same subject. We assume normal priors  $\beta_{jp} \stackrel{iid}{\sim} \mathbf{N}(0, u_\beta^2)$  with fixed  $u_\beta^2$ . In addition, we place a sum-to-zero constraint on the prior of  $\beta_{jp}$ 's corresponding to the categories of a categorical covariate, and the model ensures meaningful inference on  $\beta_{jp}$ . If desired, a joint prior distribution of  $\kappa_j$  and  $\beta_j$  can be considered. For example, we assume  $(\kappa'_j, \beta'_j)' \stackrel{iid}{\sim} \mathbf{N}(\mathbf{0}, \mathbf{V})$ , and  $\mathbf{V}$  accommodates potential association between covariates' effects on presence/absence of an OTU and their effects on the abundance of the OTU. We let  $s_{g_i,j} | u_s^2 \stackrel{iid}{\sim} \mathbf{N}(0, u_s^2)$  and  $u_s^2 \sim \text{Ga}(a_s, b_s)$ . Due to  $s_{g_i,j}$ , the marginal covariance matrix of  $\tilde{\mathbf{Y}}_i^*$  is  $\Omega = \Sigma + u_s^2 \mathbf{I}_J$ , and the marginal correlations between OTUs  $j$  and  $j'$  are  $\rho_{jj'} = \{\Sigma_{jj'} + u_s^2 \mathbf{1}(j = j')\} / \sqrt{(\Sigma_{jj} + u_s^2)(\Sigma_{j'j'} + u_s^2)} \in (-1, 1)$ . While any of parameters,  $\Sigma$ ,  $\Omega$  and  $\rho_{jj'}$ , can be considered as a measure of dependence between OTUs, we use  $\rho_{jj'}$  for easy interpretation in the simulation studies and real data analyses illustrated later.

Recall that the mean and median of  $Y_{ij}^*$  are proportional to  $\exp(r_i + \alpha_j)$ , implying that  $r_i$  and  $\alpha_j$  are not identifiable. To circumvent potential identifiability issues, we follow [Li et al. \(2017\)](#) and use the mean-constrained prior with a mixture of mixture of normals on  $r_i$  and  $\alpha_j$ ;

$$(9) \quad \begin{aligned} r_i | \psi^r, \omega^r, \xi^r &\stackrel{iid}{\sim} \sum_{l=1}^{L^r} \psi_l^r \left\{ \omega_l^r \mathbf{N}(\xi_l^r, u_r^2) + (1 - \omega_l^r) \mathbf{N} \left( \frac{v_r - \omega_l^r \xi_l^r}{1 - \omega_l^r}, u_r^2 \right) \right\}, \\ \alpha_j | \psi^\alpha, \omega^\alpha, \xi^\alpha &\stackrel{iid}{\sim} \sum_{l=1}^{L^\alpha} \psi_l^\alpha \left\{ \omega_l^\alpha \mathbf{N}(\xi_l^\alpha, u_\alpha^2) + (1 - \omega_l^\alpha) \mathbf{N} \left( \frac{v_\alpha - \omega_l^\alpha \xi_l^\alpha}{1 - \omega_l^\alpha}, u_\alpha^2 \right) \right\}, \end{aligned}$$

where  $v_r$  and  $v_\alpha$  are prespecified mean constraints for the distributions of  $r_i$  and  $\alpha_j$ , respectively.  $u_r^2$  and  $u_\alpha^2$  are fixed. Different from a multinomial model that conditions on sample total counts, our model assumes  $\mathbf{E}(Y_{ij}^* | \mu_{ij}, \Sigma) \propto \exp(\mu_{ij}) = \exp(r_i + \alpha_j + \mathbf{x}'_i \beta_j + s_{g_i,j})$  in (8), and simultaneously performs model-based normalization through random  $r_i$ 's. It flexibly accounts for compositionality in microbiome data and improves the inference on parameters of primary interest compared to a model using plug-in empirical estimates for normalizing factors ([Shuler et al., 2021](#)). To specify the value of  $v_r$ , we obtain sample scale factor estimates by the cumulative sum scaling (CSS) normalization method in [Paulson et al. \(2013\)](#), and fix  $v_r$  at the average of those estimates. Specifically, we let  $v_r = \frac{1}{N} \sum_{i=1}^N \log(\sum_{j=1}^J \mathbf{1}_{Y_{ij} \leq q_i} Y_{ij})$ , where  $q_i$  is set as the largest quantile such that the difference in quantiles across samples is small enough. Then we set  $v_\alpha = \frac{1}{NJ} \sum_{i=1}^N \sum_{j=1}^J \log(Y_{ij} + 0.01) - v_r$ . [Lee and Sison-Mangus \(2018\)](#) and [Shuler et al. \(2021\)](#) showed that overall means  $r_i + \alpha_j$  can be well estimated under the mean-constrained prior and their posterior inference is not sensitive to the choice of  $v_r$  and  $v_\alpha$ . To complete the specification of the mean-constrained prior, we place Dirichlet priors for  $\psi^\chi = (\psi_1^\chi, \dots, \psi_{L^\chi}^\chi)$  and beta priors for  $\omega_l^\chi$ ,  $\chi \in \{r, \alpha\}$ ,  $\psi^\chi \sim \text{Dir}(a_\psi^\chi, \dots, a_\psi^\chi)$  and  $\omega_l^\chi \stackrel{iid}{\sim} \text{Be}(a_\omega^\chi, b_\omega^\chi)$ , where the hyperparameters  $a_\psi^\chi$ ,  $a_\omega^\chi$  and  $b_\omega^\chi$  are fixed. Finally, we set  $\xi_l^\chi \stackrel{iid}{\sim} \mathbf{N}(\bar{\xi}^\chi, v_\chi^2)$  with fixed  $\bar{\xi}^\chi$  and  $v_\chi^2$ . With random mixture weights,  $\omega_l^\chi$  and  $\psi_l^\chi$ , and random locations  $\xi_l^\chi$ , the mixture models in (9) flexibly capture various shapes of distributions, while keeping their means at  $v_\chi$  and provide reasonable estimates of  $r_i + \alpha_j$ .

**2.2. Posterior Computation.** Let  $\theta = \{\lambda_{jk}, \phi_j, \tau_k, \kappa_{jp}, \delta_{ij}, \eta_i, \sigma^2, r_i, \alpha_j, \beta_{jp}, s_{g_i,j}, u_s^2, \omega_l^\alpha, \psi_l^\alpha, \xi_l^\alpha, \omega_l^r, \psi_l^r, \xi_l^r\}$  be a vector of all random parameters. We use Markov chain Monte Carlo (MCMC) methods to draw samples from the posterior distribution of  $\theta$ . We write a Laplace



distribution in (4) as a normal scale mixture to facilitate the posterior computation, and introduce latent mixture indicators for easy computation in updating  $\omega_l^\chi$ ,  $\psi_l^\chi$  and  $\xi_l^\chi$ ,  $\chi \in \{r, \alpha\}$ . Given the latent variables, all parameters except for  $\phi_j$  are in standard conjugate forms and can be easily updated through a data augmented Gibbs step. Details of the posterior computation are given in Supp. §1 (Shuangjie *et al.*, 2022). We examined the mixing and convergence of the Markov chains using trace plots and autocorrelation plots and did not find evidence of poor mixing or bad convergence for both the upcoming simulation examples and the real data analyses. The open-source code that implements the model is available online at <https://github.com/Zsj950708/ZI-MLN>.

### 3. Simulation Studies.

3.1. *Simulation 1.* We performed simulation studies and assessed the performance of the zero-inflated multivariate log-normal kernel model (ZI-MLN). For Simulation 1, we considered a case where no covariate is included, and each subject has one sample. We fitted a simplified model that has  $\mu_{ij} = r_i + \alpha_j + s_{g_i,j}$  and  $\epsilon_{ij} = \Phi_1(\kappa_{j0} | 0, 1)$ . The simplified model is useful in estimating the interactions between OTUs for data without covariates. We let  $J = 150$  OTUs and  $N = 20$  samples, a sample from each of  $M = 20$  subjects. For joint sparsity, we set  $K^{\text{tr}} = 5$  and generated  $e_{jk} \stackrel{iid}{\sim} \text{Ber}(g)$  with sparsity level  $g = 0.8$ . We then let  $\lambda_{jk}^{\text{tr}} = 0$  if  $e_{jk} = 1$  and otherwise, simulated  $\lambda_{jk}^{\text{tr}} \stackrel{iid}{\sim} \text{Unif}(-3, 3)$ . We let  $\Sigma^{\text{tr}} = \Lambda^{\text{tr}} \Lambda^{\text{tr},\prime} + \sigma^{2,\text{tr}} \mathbf{I}_J$  with  $\sigma^{2,\text{tr}} = 1$ . We also simulated random effects  $s_{g_i,j}^{\text{tr}} \stackrel{iid}{\sim} \text{N}(0, u_s^{2,\text{tr}})$  with  $u_s^{2,\text{tr}} = 1$ , sample size factors  $r_i^{\text{tr}} \stackrel{iid}{\sim} \text{Unif}(3, 7)$  and OTU size factors  $\alpha_j^{\text{tr}} \stackrel{iid}{\sim} \text{Unif}(0, 2)$ . We then simulated  $\mathbf{Y}_i^{*,\text{tr}} \stackrel{indep}{\sim} \text{log-N}_J(r_i^{\text{tr}} \mathbf{1}_J + \boldsymbol{\alpha}^{\text{tr}} + \mathbf{s}_i^{\text{tr}}, \Sigma^{\text{tr}})$ . For excess zeros, we generated  $\kappa_{j0}^{\text{tr}} \stackrel{iid}{\sim} \text{Unif}(-1, 0)$  and simulated  $\delta_{ij}^{\text{tr}} | \epsilon_j^{\text{tr}} \stackrel{indep}{\sim} \text{Ber}(\epsilon_j^{\text{tr}})$  with  $\epsilon_j^{\text{tr}} = \Phi_1(\kappa_{j0}^{\text{tr}} | 0, 1)$ . We then let  $Y_{ij} = 0$  if  $\delta_{ij}^{\text{tr}} = 1$  and otherwise, let  $Y_{ij} = \lfloor Y_{ij}^{*,\text{tr}} \rfloor$ . It yielded approximately 40% of  $Y_{ij}$  being 0. The lower left triangle of the heatmap in Fig 1(a) illustrates the true marginal correlation matrix  $\rho_{jj'}^{\text{tr}} = \{\Sigma_{jj'}^{\text{tr}} + u_s^{2,\text{tr}} \mathbf{1}(j = j')\} / \sqrt{(\Sigma_{jj}^{\text{tr}} + u_s^{2,\text{tr}})(\Sigma_{j'j'}^{\text{tr}} + u_s^{2,\text{tr}})}$ . Empirical correlation estimates  $\rho_{jj'}^{\text{em}}$  are computed using transformed raw counts and illustrated in Supp. Fig 2(a) (Shuangjie *et al.*, 2022). It shows that naive correlation estimates are noisy and do not capture the true interrelationship between OTUs.

To fit the model, we set the fixed hyperparameters as follows; For the mean-constrained priors of  $r_i$  and  $\alpha_j$ , we let  $L^r = 5, L^\alpha = 10$ ,  $a_\psi^r = a_\psi^\alpha = 1$ , and  $a_\omega^r = b_\omega^r = a_\omega^\alpha = b_\omega^\alpha = 5$ . The values of the mean constraints  $v^r$  and  $v^\alpha$  were specified through the empirical approach described in § 2.1. We set the prior mean and variance of  $\kappa_{j0}$ ,  $\bar{\kappa}_0 = 0$  and  $u_\kappa^2 = 3$ . Also, we set  $a_\sigma = b_\sigma = 3$  and  $a_s = b_s = 1$ . Lastly, we set  $K = 10$ ,  $a_\phi = 1/2$ ,  $a_\tau = 1$  and  $b_\tau = 1/50$ . We simulated posterior samples through MCMC described in § 2.2. We discarded the first 15,000 draws for burn-in and kept the next 15,000 draws for posterior inference. It took 25 minutes for every 5,000 iterations on a M1 Mac. Assessment of MCMC simulation convergence is discussed in Supp. §2.1 (Shuangjie *et al.*, 2022). We also checked the posterior distributions of  $\tau_k$  to examine if a greater value of  $K$  is needed. The posterior distributions of some  $\tau_k$ 's are greatly concentrated close to zero, indicating that  $K = 10$  is sufficiently large for the dataset. We also performed sensitivity analyses to the specification of  $a_\phi$  and  $b_\tau$  to examine the robustness of the model in estimating  $\Sigma$ .

Posterior inference on the marginal correlations  $\rho_{jj'}$  is illustrated in Fig 1. The heatmap in panel (a) compares posterior mean estimates  $\hat{\rho}_{jj'}$  in the upper right triangle to their truth  $\rho_{jj'}^{\text{tr}}$  in the lower left triangle. Panel (b) shows a histogram of the differences  $\hat{\rho}_{jj'} - \rho_{jj'}^{\text{tr}}$ ,  $j < j'$ . In the histogram, the differences are tightly centered around 0, indicating that the method

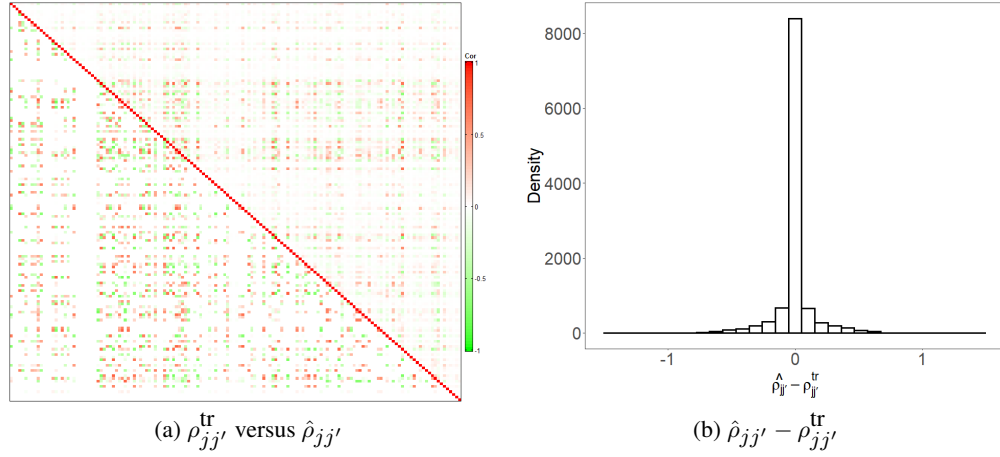


FIG 1. [Simulation 1] The upper right and lower left triangles of the heatmap in panel (a) illustrate posterior estimates of correlations  $\hat{\rho}_{jj'}$  and their true values  $\rho_{jj'}^{\text{tr}}$ , respectively. Panel (b) has a histogram of differences between  $\hat{\rho}_{jj'}$  and  $\rho_{jj'}^{\text{tr}}$ .

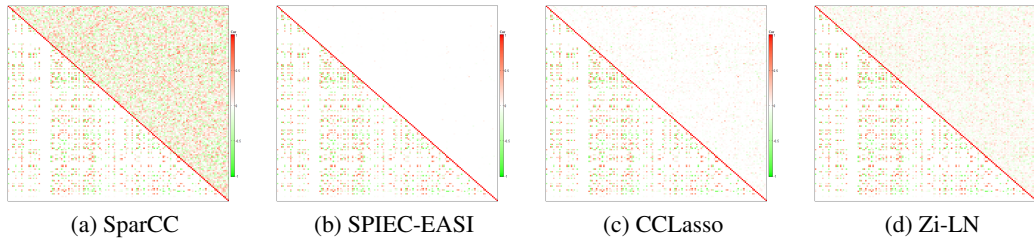


FIG 2. [Simulation 1: Comparison] The upper right and lower left triangles of each heatmap illustrate estimates  $\hat{\rho}_{jj'}$  of correlations between OTUs and their true values  $\rho_{jj'}^{\text{tr}}$ , respectively. Panels (a)-(d) are for SparCC, SPIEC-EASI, CCLasso and Zi-LN, respectively.

provides good estimates of the correlations. Our method identifies the truly inactive OTUs successfully, and the true OTU interrelationship structure is reasonably well captured even when the sample size is much smaller than the number of OTUs ( $N = 20$  and  $J = 150$ ), and excess zeros are present. Supp. Fig 3 (Shuangjie *et al.*, 2022) compares posterior mean estimates of baseline abundances  $r_i + \alpha_j$  and probabilities  $\epsilon_{ij}$  of an OTU being absent to their truth. In the figure, the absence/presence of OTUs and OTU baseline abundances are well estimated, which provides a crucial basis for the estimation of the parameters of primary interest, such as  $\Sigma$ . We performed posterior predictive checking to examine model fit under ZI-MLN. Fig 4(a) compares posterior predictive median estimates  $\hat{y}_{ij}^{\text{pred}}$  of OTU counts to the observed counts  $y_{ij}$  and shows that our model provides a good model fit to the data.

For comparison, we applied SparCC (Friedman and Alm, 2012), SPIEC-EASI (Kurtz *et al.*, 2015), CCLasso (Fang *et al.*, 2015) and Zi-LN (Prost, Gazut and Brüls, 2021) that are briefly described in § 1. The comparators infer dependence structure between OTUs through the estimation of covariance or precision matrix under some sparsity assumptions and yield correlation estimates  $\hat{\rho}_{jj'}$ . The tuning parameter for sparsity in SparCC, SPIEC-EASI and Zi-LN is chosen by cross-validation.  $\hat{\rho}_{jj'}$  under the comparators are compared to the true values  $\rho_{jj'}^{\text{tr}}$ , in Fig 2. Fig 3 illustrates histograms of differences  $\hat{\rho}_{jj'} - \rho_{jj'}^{\text{tr}}$ . Root mean square error (RMSE) for  $\rho_{jj'}, j < j'$  for the models including ZI-MLN is shown in Tab 1(a). ZI-MLN outperforms in recovering the dependence structure between OTUs. Poor performance of the comparators can be because they do not account for overdispersion and/or excess zeros and/or they lack flexible normalization for compositionality. In addition, we compare our

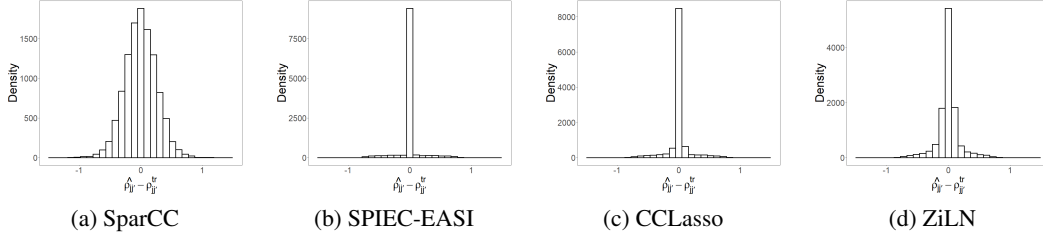


FIG 3. [Simulation 1: Comparison] A histogram of differences between  $\hat{\rho}_{jj'}$  under SparCC, SPIEC-EASI, CCLasso and Zi-LN and  $\rho_{jj'}^r$ , in panels (a)-(d), respectively.

TABLE 1

[Simulation 1: Comparison] RMSEs are computed for correlations  $\rho_{jj'}, j < j'$ , binary indicator  $\delta_{ij}$  of an OTU being absent in a sample and mean abundance  $\mu_{ij}$  under ZI-MLN and comparators.

Model	$\rho_{jj'}$
ZI-MLN	<b>0.129</b>
SparCC	0.258
SPIEC-EASI	0.167
CCLasso	0.166
Zi-LN	0.173

(a)  $\rho_{jj'}$

Model	$\delta_{ij}$	$\mu_{ij}$
ZI-MLN	<b>0.084</b>	<b>0.449</b>
ZI-MLN without $\Lambda$	0.088	0.543
MetagenomeSeq	0.095	1.717

(b)  $\delta_{ij}$  and  $\mu_{ij}$

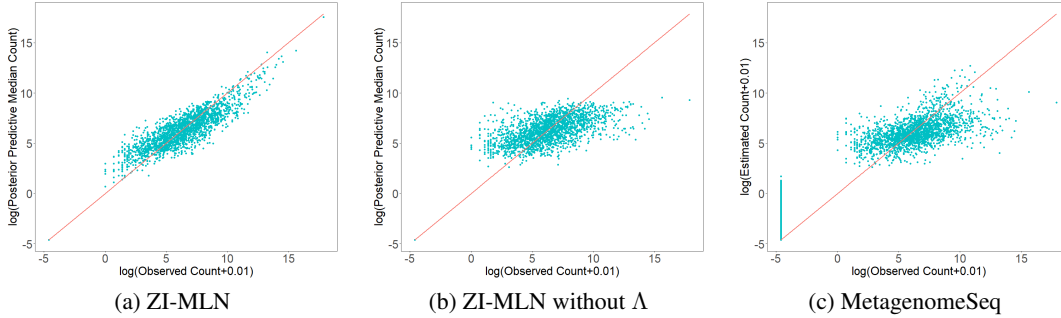


FIG 4. [Simulation 1] Scatter plots of observed  $\log(y_{ij} + 0.01)$  versus  $\log(\hat{y}_{ij}^{pred} + 0.01)$  estimated by ZI-MLN with  $\Lambda$  and ZI-MLN without  $\Lambda$  are shown in panels (a) and (b), respectively.  $\hat{y}_{ij}^{pred}$  is the median estimate of the posterior predictive distribution. Panel (c) is the scatter plots of observed  $\log(y_{ij} + 0.01)$  versus  $\log(\hat{\mu}_{ij} + 0.01)$ , where  $\hat{\mu}_{ij}$  are mean abundances of OTUs estimated by metagenomeSeq.

method to ZI-MLN without  $\Lambda$ , a simpler version of our ZI-MLN, and metagenomeSeq in Paulson *et al.* (2013) for comparison of the estimation of  $\mu_{ij}$  and  $\delta_{ij}$ . We simplified our ZI-MLN by letting  $\Sigma = \sigma^2 I_J$  and kept the remaining model components including zero-inflation and subject-specific random effects the same. We call it ‘‘ZI-MLN without  $\Lambda$ .’’ MetagenomeSeq is a likelihood-based model that uses transformed counts  $\log_2(y_{ij} + 1)$  and assumes a zero-inflated normal mixture model separately for individual OTUs, where the mean has a regression function of covariates, a sample size factor fixed at estimates by CSS normalization method and an OTU size factor similar to ZI-MLN. Under metagenomeSeq, the zero inflation probabilities of  $y$  are common for all OTUs in a sample and regressed on the sample total counts through a logit link. An EM algorithm is used to estimate unknown parameters.

The additional comparators do not account for the interrelationships between OTUs and do not provide any inference on OTU interaction. We compared parameter estimates of  $\mu_{ij}$  and  $\delta_{ij}$  under each of the three models, including ZI-MLN, to the truth and computed RMSE for the parameters, summarized in Tab 1(b). The table shows that our model outperforms the comparators in the estimation of OTU mean abundances and absence/presence. Especially, comparison to ZI-MLN without  $\Lambda$  indicates that ignoring the dependence structure among counts when it is present can deteriorate the inference on the other parameters, including  $\mu_{ij}$ . It is also indicated from posterior predictive checking under ZI-MLN without  $\Lambda$  shown in Fig 4(b). Comparison of mean abundance estimates  $\hat{\mu}_{ij}$  by metegenomSeq to observed counts in Fig 4(c) also shows potential model misfit under metagenomeSeq.

**3.2. Simulation 2.** We conducted Simulation 2 for a case having covariates. We examined the estimation of covariate effects on OTU abundances and their presence/absence in addition to the estimation of  $\Sigma$ . We set the number of OTUs  $J = 150$  and assumed two samples from each of  $M = 35$  subjects under two experimental conditions. We thus have the number of samples  $N = 70$  and  $g_i \in \{1, \dots, M\}$  with  $n_{g_i} = 2$  for all  $g_i$ . The remaining setup is similar to that of Simulation 1. We set  $K^{\text{tr}} = 5$ ,  $\sigma^{2,\text{tr}} = 1$  and  $u_s^{2,\text{tr}} = 1$ , and simulated  $\lambda_{jk}^{\text{tr}}$ ,  $r_i^{\text{tr}}$ ,  $\alpha_j^{\text{tr}}$  and  $s_{g_i,j}^{\text{tr}}$ , as done in Simulation 1. We included a binary covariate that represents the experimental conditions using a pair of dummy variables  $(x_{i1}, x_{i2}) \in \{(1, 0), (0, 1)\}$ . The corresponding coefficients  $\beta_{j1}$  and  $\beta_{j2}$  thus quantify changes in mean abundance by a condition compared to the overall mean abundance  $r_i^{\text{tr}} + \alpha_j^{\text{tr}}$ . In addition, we included a continuous covariate,  $x_{i3}$  generated from  $N(0, 1)$ , so we have  $\mathbf{x}_i = (x_{i1}, x_{i2}, x_{i3})'$  with  $P = 3$ . For the coefficients, we set  $\beta_{jp}^{\text{tr}} \stackrel{iid}{\sim} N(0, 1)$  for  $p = 1, \dots, P$ . For  $\epsilon_{ij}$ , we let  $\tilde{\mathbf{x}}_i = (x_{i2}, x_{i3})'$  with  $P_\kappa = 2$  using  $x_{i1}$  as a reference category, and simulated  $\kappa_{jp}^{\text{tr}} \stackrel{iid}{\sim} \text{Unif}(-0.5, 0)$ ,  $p = 0, \dots, P_\kappa$ . We finally generated counts  $Y_{ij}$  as follows; we simulated  $\mathbf{Y}_i^{*,\text{tr}} \stackrel{indep}{\sim} \log\text{-N}_J(r_i^{\text{tr}} \mathbf{1}_J + \boldsymbol{\alpha}^{\text{tr}} + \mathbf{x}_i' \boldsymbol{\beta}^{\text{tr}} + \mathbf{s}_i^{\text{tr}}, \Sigma^{\text{tr}})$ , with  $\Sigma^{\text{tr}} = \Lambda^{\text{tr}} \Lambda^{\text{tr},\prime} + \sigma^{2,\text{tr}} \mathbf{I}_J$  and  $\boldsymbol{\beta}^{\text{tr}}$  being a  $J \times P$  matrix of  $\beta_{jp}^{\text{tr}}$ . We also generated binary indicators  $\delta_{ij}^{\text{tr}} \mid \epsilon_{ij}^{\text{tr}} \stackrel{indep}{\sim} \text{Ber}(\epsilon_{ij}^{\text{tr}})$  with  $\epsilon_{ij}^{\text{tr}} = \Phi(\kappa_{j0}^{\text{tr}} + \kappa_j^{\text{tr},\prime} \tilde{\mathbf{x}}_i \mid 0, 1)$ . We then let  $Y_{ij} = 0$  if  $\delta_{ij}^{\text{tr}} = 1$ , and let  $Y_{ij} = \lfloor Y_{ij}^{*,\text{tr}} \rfloor$ , otherwise. The simulated dataset has approximately 40% of counts being zero. Fig 5(a) and Supp. Fig 5(a) (Shuangjie *et al.*, 2022) illustrate the true marginal correlations  $\rho_{jj'}^{\text{tr}}$  and their naive empirical estimates  $\rho_{jj'}^{\text{em}}$  using transformed counts after the normalization, respectively.

We specified the fixed hyperparameter values similar to those in Simulation 1. We set  $L^r = 8$  due to a larger sample size. We set  $u_\beta^2 = 25$  for the prior of  $\beta_{jp}$  and placed the sum-to-zero constraint for  $\beta_{j1}$  and  $\beta_{j2}$  for identifiability. We set  $\bar{\kappa}_p = 0$  for all  $p$  and  $u_\kappa^2 = 3$ . The MCMC simulation was run over 30,000 iterations, with the first 15,000 iterations discarded as burn-in. A discussion on the chain's convergence and mixing is in Supp. §2.2 (Shuangjie *et al.*, 2022). It took 0.7 hours on average for every 5,000 iterations on a M1 Mac.

Fig 5 illustrates posterior mean estimates  $\hat{\rho}_{jj'}$  of marginal correlations between OTUs  $j$  and  $j'$ ,  $j \neq j'$ . The figure shows that the underlying interrelationships between OTUs are well captured even with small sample size and excess zero counts. The histogram in panel (b) shows the differences  $\hat{\rho}_{jj'} - \rho_{jj'}^{\text{tr}}$  are close to zero. Figs 6(a)-(b) and Supp. Figs 6(a)-(c) (Shuangjie *et al.*, 2022) compare regression coefficient estimates,  $\hat{\beta}_{jp}$  and  $\hat{\kappa}_{jp}$  to their true values. From Figs 6(a)-(b), posterior mean estimates of  $\beta_{j1} - \beta_{j2}$  and  $\beta_{j3}$  are close to the true values. Here,  $\beta_{j1} - \beta_{j2}$  quantifies the difference in the mean abundances between two categories of the binary covariate. Their posterior 95% credible intervals capture the truth well. Supp. Fig 7 (Shuangjie *et al.*, 2022) shows that posterior estimates  $\hat{r}_i + \hat{\alpha}_j$  and  $\hat{\epsilon}_{ij}$  are also close to their true values. To check the model fit, we compare median estimates  $\hat{y}_{ij}^{\text{pred}}$  of

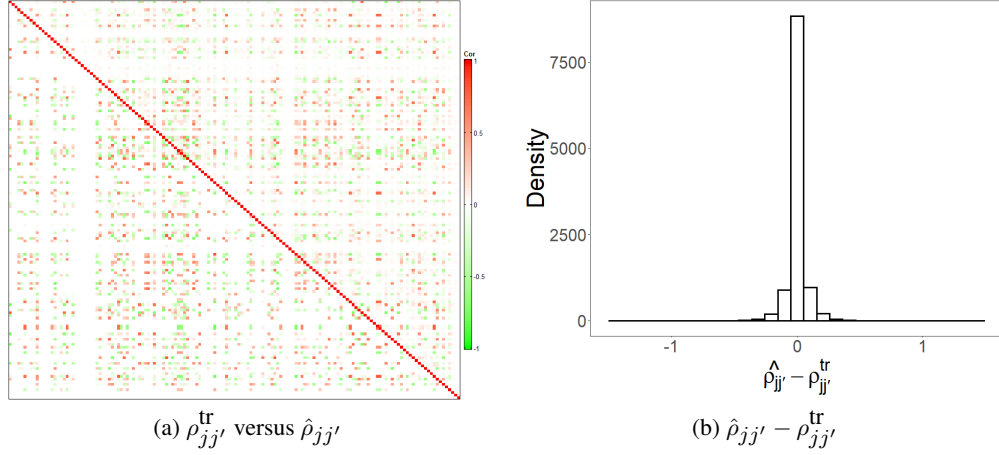


FIG 5. [Simulation 2] The upper right and lower left triangles of the heatmap in panel (a) illustrate posterior estimates of correlations  $\hat{\rho}_{jj'}$  and the true values of the correlations  $\rho_{jj'}^{\text{tr}}$ , respectively. Panel (b) has a histogram of differences between  $\hat{\rho}_{jj'}$  and  $\rho_{jj'}^{\text{tr}}$ .

TABLE 2

[Simulation 2: Comparison] RMSEs are computed for  $\rho_{jj'}, j < j', \delta_{ij}, \mu_{ij}, \beta_{j2} - \beta_{j1}, \beta_{j3}$  and  $\kappa_{jp}$  under ZI-MLN and comparators.

Model	$\rho_{jj'}$	Model	$\delta_{ij}$	$\mu_{ij}$	$\beta_{j2} - \beta_{j1}$	$\beta_{j3}$	$\kappa_{j0}$	$\kappa_{j1}$	$\kappa_{j2}$
ZI-MLN	<b>0.063</b>	ZI-MLN	<b>0.096</b>	<b>1.084</b>	<b>0.570</b>	<b>0.359</b>	<b>0.214</b>	<b>0.183</b>	<b>0.335</b>
SparCC	0.176	ZI-MLN without $\Lambda$	0.123	1.172	0.750	0.426	0.234	0.191	0.361
SPIEC-EASI	0.158	MetagenomeSeq	0.130	1.962	1.409	0.843	-	-	-
CCLasso	0.155	EdgeR	-	2.205	0.902	0.585	-	-	-
Zi-LN	0.157								

(a)  $\rho_{jj'}$

(b)  $\delta_{ij}, \mu_{ij}, \beta_{j2} - \beta_{j1}, \beta_{j3}$  and  $\kappa_{jp}$

the posterior predictive distributions to the observed counts. Fig 6(c) provides evidence for a good model fit under ZI-MLN.

For comparison, we applied the four comparators that provide estimates of associations between OTUs, SparCC, SPIEC-EASI, CCLasso and Zi-LN, to the simulated data. The heatmaps in Fig 7 and histograms in Fig 8 compare their estimates  $\hat{\rho}_{jj'}$  to the truth  $\rho_{jj'}^{\text{tr}}$ . RMSE for  $\rho_{jj'}$  are computed for comparison between the models including ZI-MLN. Tab 2(a) shows that ZI-MLN outperforms the comparators in estimating the dependencies between OTUs. Note that the comparators do not account for covariate effects, potentially resulting in poor performance. Also, we applied three other comparators, ZI-MLN without  $\Lambda$ , metagenomeSeq and edgeR (Robinson, McCarthy and Smyth, 2010) and compared the abundance and absence/presence related model parameters. EdgeR is a likelihood-based method that uses a negative binomial generalized linear regression approach for the analysis of HTS data. It uses the normalization factors estimated by an empirical Bayes strategy and does not account for excess zeros. Similar to ZI-MLN without  $\Lambda$  and metagenomeSeq, edgeR does not account for the dependence structure among OTUs and does not provide inferences on the relationship among OTUs. MetagenomeSeq and edgeR require selecting a category of a discrete covariate as a reference category, and their  $\beta_{jp}$ 's estimate changes in the mean abundance relative to that in the reference category. We chose  $x_{i1}$  as the reference for those

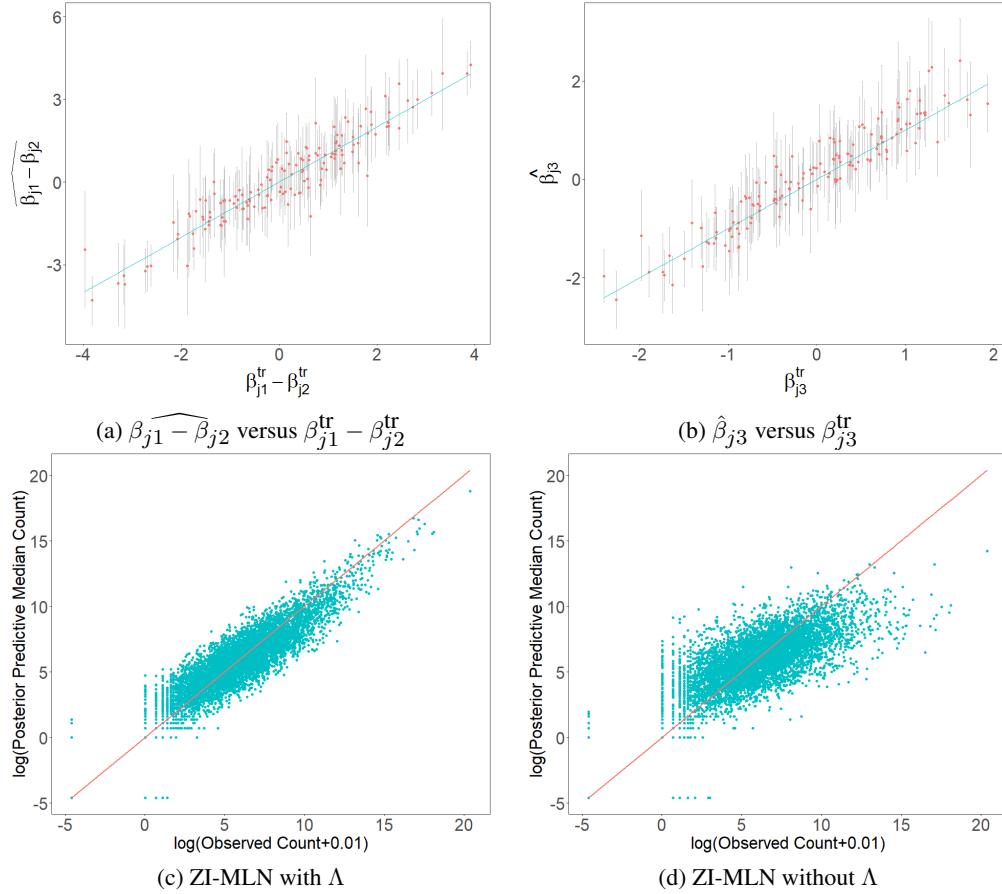


FIG 6. [Simulation 2] Panels (a) and (b) compare posterior estimates of regression coefficients  $\widehat{\beta_{j1} - \beta_{j2}}$  and  $\widehat{\beta_{j3}}$  to the truth  $\beta_{j1}^{tr} - \beta_{j2}^{tr}$  and  $\beta_{j3}^{tr}$ , respectively, where the vertical lines represent 95% credible intervals. Panels (c) and (d) compare posterior predictive median count estimates to their observed counts on the logarithm scale,  $\log(y_{ij} + 0.01)$  versus  $\log(\hat{y}_{ij}^{pred} + 0.01)$ . ZI-MLN with  $\Lambda$  and ZI-MLN without  $\Lambda$  are used in panels (c) and (d), respectively.

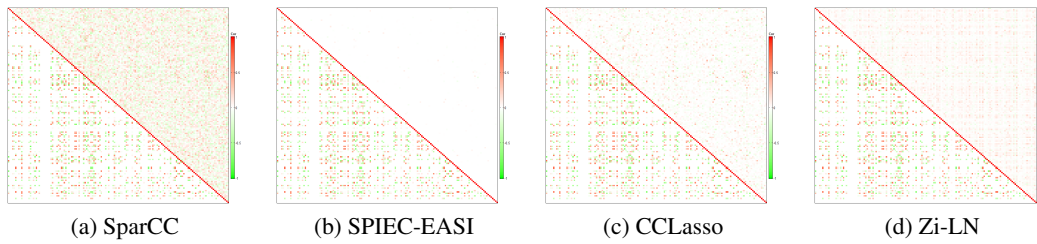


FIG 7. [Simulation 2: Comparison] The upper right and lower left triangles of each heatmap illustrate estimates  $\hat{\rho}_{j,j'}$  of correlations between OTUs and their true values  $\rho_{j,j'}^{tr}$ , respectively. Panels (a)-(d) are for SparCC, SPIEC-EASI, CCLasso and Zi-LN, respectively.

methods. Supp. Figs 6(d)-(f) and 8 (Shuangjie *et al.*, 2022) compare estimates of  $\beta_{jp}$  and  $\kappa_{jp}$  under the comparators to the truth. RMSE for each of the four models, including ZI-MLN, is computed and summarized in Tab 2(b). RMSE of  $\kappa_{jp}$  is not computed for metagenomeSeq since it has a logit regression of  $\epsilon_{ij}$  on the total sample count, but not on covariates. The results show that our model outperforms the comparators in the estimation of the parameters,  $\delta_{ij}$ ,  $\mu_{ij}$ ,  $\beta_{jp}$  and  $\kappa_{jp}$ . We also performed posterior predictive checking for ZI-MLN without



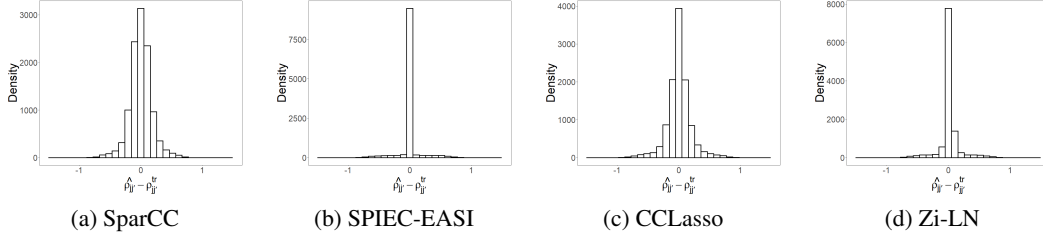


FIG 8. [Simulation 2: Comparison] A histogram of differences between  $\hat{\rho}_{jj}$  under SparCC, SPIEC-EASI, CCLasso and ZiLN and  $\rho_{jj}^{\text{tr}}$ , in panels (a)-(d), respectively.

$\Lambda$  by comparing  $\hat{y}_{ij}^{\text{pred}}$  under the model to the observed counts. As shown in Fig 6(d), ZI-MLN without  $\Lambda$  provides a poor fit to the data. Their posterior mean estimates of  $\sigma^2$  and  $u_s^2$  are greatly inflated compared to their true value. Estimates  $\hat{\sigma}^2$  and  $\hat{u}_s^2$  are 3.86 and 0.77, respectively, while their true values are  $\sigma^{2,\text{tr}} = 1$  and  $u_s^{2,\text{tr}} = 1$ . The comparison of the inference under ZI-MLN to that under ZI-MLN without  $\Lambda$  shows the necessity of modeling the dependence structure between OTUs to enhance the inference on the other parameters such as covariate effects when the interactions between OTUs are present. Estimates of the mean abundances under metagenomeSeq and edgeR are compared to the observed counts in Supp. Fig 9 (Shuangjie *et al.*, 2022).

*Additional Simulations.* We conducted additional simulation studies, Simulations 3-5 to examine the performance of our model under various settings. In Simulation 3, we first generated correlated mean vectors  $\tilde{\mu}_i^{\text{tr}} = (\tilde{\mu}_{i1}^{\text{tr}}, \dots, \tilde{\mu}_{iJ}^{\text{tr}})$  from a multivariate normal distribution and simulated OTU counts from zero-inflated Poisson distributions with means  $\exp(\tilde{\mu}_{ij}^{\text{tr}})$ . The simulation results show that our model provides reasonable estimates of the parameters even when the simulation truth is different from the assumed model, showing the robustness of the model. Importantly, the OTU interaction structure is also reasonably well reconstructed even when the dependency is embedded in the mean abundances, and the sampling distribution is incorrectly specified. In Simulation 4, we kept the simulation setup the same as in Simulation 2, but let  $\Sigma^{\text{tr}} = \sigma^{2,\text{tr}} \mathbf{I}_J$ , i.e., OTU counts are independent given the mean parameters. Although the simulation truth is closer to the assumption made under ZI-MLN without  $\Lambda$ , the results show that ZI-MLN performs almost the same as well. For Simulation 5, we used SparseDOSSA in Ma *et al.* (2021) to simulate a dataset. SparseDOSSA takes a real microbiome dataset as an input, estimates some input parameters of their data-generating model, and generates a realistic microbiome dataset that has a dependence structure between OTUs using the estimates. We used the skin microbiome dataset in § 4.1 as an input dataset. An open-source software, *SparseDOSSA2* is provided by the authors. SparseDOSSA estimates a precision matrix, one of the input parameters, with  $\ell_1$  penalty for sparsity. The sparsity assumption is similar to that under some of the comparators, SPIEC-EASI and CCLasso. It simulates count vectors from a multinomial distribution conditioning random total counts. The dataset in the scenario was thus simulated from a model significantly different from ZI-MLN. The results greatly demonstrate the robustness of ZI-MLN. The model-based normalization appropriately accounts for differences in total counts. More importantly, the model does a good job of capturing the dependence between OTUs in the truth and recovers the truly underlying between-OTU structure reasonably well. In all simulation studies, the results also show that our model compares very favorably relative to the comparators for estimation of covariate effects and of dependence structure between OTUs. More details of Simulations 3- 5 are in Supp. §2.3-2.5 (Shuangjie *et al.*, 2022), respectively. In addition, we assumed a different sparsity level for  $\Lambda^{\text{tr}}$  by generating  $e_{jk} \stackrel{iid}{\sim} \text{Ber}(g)$  with  $g = 0.5$ , and reran analyses under the settings of Simulations 1-4. The results show that ZI-MLN recovers the truth

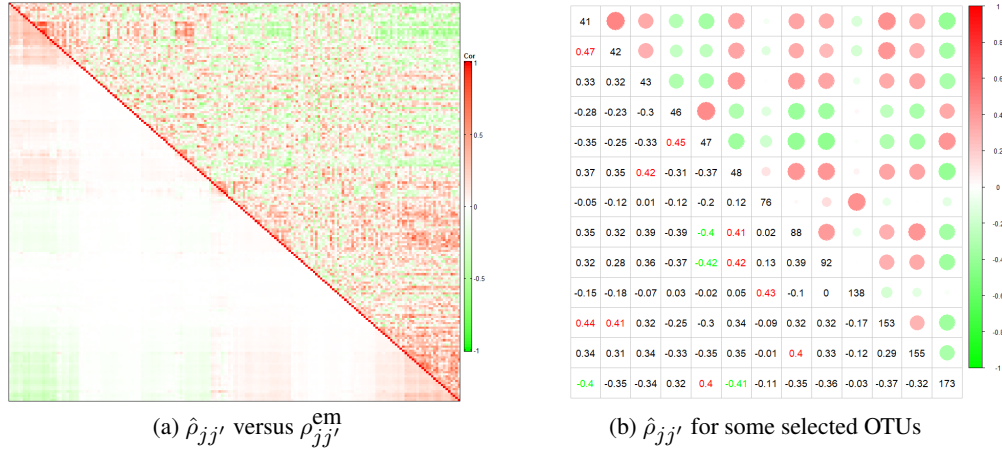


FIG 9. [Skin Microbiome Data] Posterior correlation estimates  $\hat{\rho}_{jj'}$  (lower left triangle) and empirical correlation estimates  $\rho_{jj'}^{\text{em}}$  (upper right triangle) are shown in panel (a). Panel (b) have the OTUs having  $|\hat{\rho}_{j,j'}| \geq 0.40$  for any  $j' \neq j$ .

well with a lower sparsity level and works better than the comparators under the comparison metrics.

#### 4. Real Data Analyses.

4.1. *Skin Microbiome Data.* We applied our ZI-MLN to a subset of the chronic wound microbiome data in Verbanic *et al.* (2020). The study was conducted to investigate the effect of debridement on the wound microbial community. Skin swab samples were collected under three conditions, healthy skin, pre-debridement, and post-debridement conditions. The skin microbiome dataset was analyzed Shuler *et al.* (2021), which showed changes in the community-level microbial richness and abundance diversity by the experimental conditions. For an illustration of ZI-MLN without covariates, we used a subset of the data that consists of  $N = 20$  healthy skin samples collected from  $M = 20$  subjects and investigated the interaction structure between OTUs in the healthy skin samples. We removed OTUs that have zero counts in more than 50% of the samples, leaving  $J = 187$  OTUs for analysis. The threshold of 50% was chosen so that each OTU has at least 10 nonzero counts, and the model parameters such as  $\alpha_j$  can be reliably estimated. Manual inspection of the curated OTU list indicated that the threshold chosen did not eliminate OTUs of major biological importance. In addition, we performed sensitivity analysis to the specification of the threshold. We found that any reasonable choice has little impact on the posterior inference, showing robustness of our model. Details of the sensitivity analysis are summarized in Supp. §3.1 (Shuangjie *et al.*, 2022). Fig 9(a) shows empirical correlation estimates  $\rho_{jj'}^{\text{em}}$  computed using  $\log(y_{ij} + 0.01)$  after normalization with CSS sample size factor estimates. To fit ZI-MLN, the values of the fixed hyperparameter values were set similar to those of Simulation 1 in § 3.1. The MCMC simulation was run over 30,000 iterations, with the first 15,000 iterations discarded as burn-in. It took 25 minutes for every 5,000 iterations on a M1 Mac.

Fig 9(a) illustrates posterior mean estimates  $\hat{\rho}_{jj'}$  of the marginal correlations for all OTUs. From panel (a), correlation estimates are overall small for most of  $(j, j')$ , implying weak interactions between OTUs. Compared to  $\rho_{jj'}^{\text{em}}$ ,  $\hat{\rho}_{jj'}$ 's are shrunken toward zero for many OTUs. The overall weak correlations among OTUs in the skin samples are consistent with previous analysis. Specifically, Bashan *et al.* (2016) analyzed data from the Human Microbiome Project and the Student Microbiome Project, and compared samples from the gut and

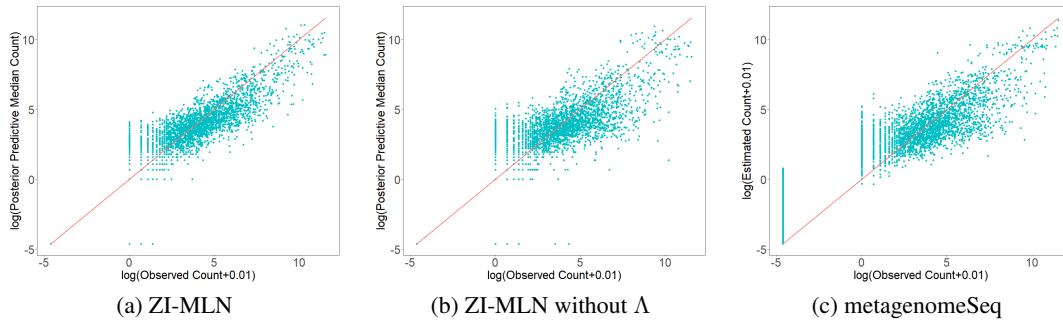


FIG 10. [Skin Microbiome Data: Comparison] Panels (a) and (b) have scatter plots of observed  $\log(y_{ij} + 0.01)$  versus  $\log(\hat{y}_{ij}^{\text{pred}} + 0.01)$  under ZI-MLN and ZI-MLN without  $\Lambda$ , respectively. Panel (c) is the scatter plots of observed  $\log(y_{ij} + 0.01)$  versus mean abundance estimates  $\log(\hat{\mu}_{ij} + 0.01)$  by metagenomeSeq.

oral microbiome to those from the skin microbiome. They reported that, while the gut and mouth microbiome samples appeared to exhibit universal dynamics of inter-species interactions, the extent of such interactions in the skin microbiome samples was relatively low. Fig 9(b) presents  $\hat{\rho}_{jj'}$  for the OTUs that have  $|\hat{\rho}_{jj'}| \geq 0.40$  for any  $j' \neq j$ , where the value of 0.4 is arbitrarily chosen to make the estimates readable. Taxonomic information of the OTUs in Fig 9(b) is given in Supp. Tab 4 (Shuangjie *et al.*, 2022). From panel (b) and the supp. table 4 (Shuangjie *et al.*, 2022), OTUs 43 and 88 belonging to genera *Porphyromonas* and *Peptoniphilus*, respectively, are estimated to be positively correlated with  $\hat{\rho} = 0.39$ . Interestingly, they were found to co-occur in a large sample of genitourinary microbiome samples (Qin *et al.*, 2021) as well as vaginal samples (Xiaoming *et al.*, 2021) and were suggested to be ‘keystone’ species, i.e., strongly interacting species that help define their ecological system. These species are also found to co-occur in skin samples (Chattopadhyay *et al.*, 2021), where they are more abundant in patients with diabetic foot ulcers (Park *et al.*, 2019). OTUs 43 and 48 having correlation estimate  $\hat{\rho} = 0.42$  belong to genera *Porphyromonas* and *Campylobacter*, respectively, that are both potentially pathogenic. *Porphyromonas* is a known pathogenic genus in periodontitis and is a risk factor in inflammatory bowel disease, while *Campylobacter* is a known gut and oral pathogen with a role in inflammatory bowel disease. Their positive correlation estimate may reflect a tendency to co-occur, as both are observed in inflammatory bowel disease (Cai *et al.*, 2021). From Supp. Tab 4 (Shuangjie *et al.*, 2022), OTUs that have a large positive value of  $\hat{\rho}_{jj'}$  tend to be phylogenetically closely related. For example, OTUs 41 and 42 having  $\hat{\rho} = 0.47$  belong to the same order *Micrococcales*. Similarly, OTUs 46 and 47 with  $\hat{\rho} = 0.45$  having are in family *Chitinophagaceae*. On the other hand, some OTUs are estimated to have a positive association with phylogenetically distant OTUs. For example, the correlation estimates between OTU 153 and OTUs 41 and 42 are  $\hat{\rho} = 0.44$  and 0.41, respectively, but OTU 153 is not phylogenetically closely related to OTUs 41 and 42. Interestingly, OTU 153 has similar interaction patterns with OTUs 41 and 42 in the same genus. Fig 10(a) has a scatter plot comparing the posterior predictive median estimates  $\hat{y}_{ij}^{\text{pred}}$  to the observed counts. The posterior predictive checking indicates a good model fit by ZI-MLN.

We also applied the comparators, SparCC, SPIEC-EASI, CCLasso and Zi-LN to the skin microbiome data for comparison. Their correlation estimates  $\hat{\rho}_{jj'}$  are illustrated in Fig 11 with the naive estimates of the correlations. SPIEC-EASI and CCLasso produce  $\hat{\rho}_{jj'}$  very close or equal to zero for most OTU pairs, while SparCC has nonzero estimates for a majority of  $\rho_{jj'}$ . In addition, ZI-MLN without  $\Lambda$  and metagenomeSeq are applied for further comparison. In Fig 10(b), the posterior predictive median estimates  $\hat{y}_{ij}^{\text{pred}}$  under ZI-MLN

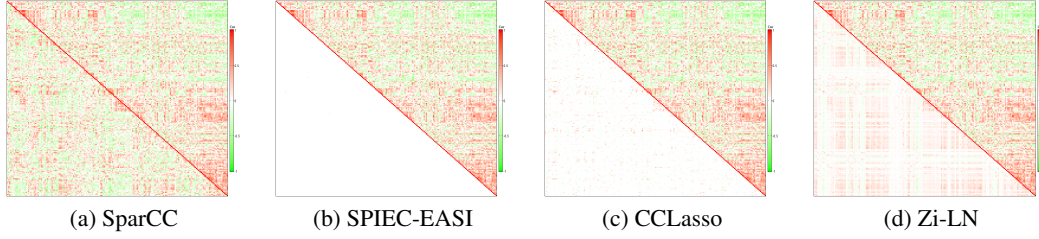


FIG 11. [Skin Microbiome Data: Comparison] Correlation estimates  $\hat{\rho}_{jj'}$  (lower left triangle) and empirical correlation estimates  $\rho_{jj'}^{em}$  (upper right triangle) are shown. The estimates in panel (a)-(d) are obtained by SparCC, SPIEC-EASI, CCLasso and Zi-LN, respectively.

without  $\Lambda$  are compared to the observed counts. In panel (c), mean abundance estimates under metagenomeSeq are compared to the observed counts. A comparison of those plots to that in panel (a) indicates that our ZI-MLN provides a better model fit, possibly because our model accounts for microbial interactions.

**4.2. Human Gut Microbiome Data.** We analyzed the microbiome dataset available from the inflammatory bowel disease (IBD) multi-omics database (<https://ibdmdb.org/>) with our ZI-MLN. Crohn’s disease (CD) and ulcerative colitis (UC) are the most prevalent forms of IBD and are characterized by chronic inflammation of the gastrointestinal tract. As part of the Integrative Human Microbiome Project (iHMP), [Lloyd-Price \*et al.\* \(2019\)](#) conducted an integrated study of multiple molecular features of the gut microbiome to investigate host- and microbiome-specific taxonomic and molecular features related to IBD and how they vary over time. In the study, biopsies were taken during the initial screening colonoscopy from the participants who were recruited from multiple medical centers and sequenced using 16S rRNA gene amplicon sequencing. For an illustration of our statistical model, we used part of their 16S rRNA sequencing data. In particular, we included the samples obtained from 37 pediatric participants from two recruitment sites, Cincinnati Children’s Hospital and Massachusetts General Hospital (MGH) Pediatrics. For some subjects, two samples were collected from different biopsy locations, resulting in a total of 67 samples. In addition to biopsy locations, we included one continuous covariate, age and five categorical covariates such as sex, race, recruitment site and disease phenotype. Disease phenotype is a trinary covariate taking a value of UC, CD or non-IBD, and the others are binary, resulting in  $P = 12$  after adding dummy variables to indicate the categories of the discrete covariates. Supp. Tab 5 ([Shuangjie \*et al.\*, 2022](#)) lists all covariates with their supports. We removed OTUs having zero count in more than 80% of the samples or average counts smaller than five.  $J = 107$  OTUs are left after the preprocessing. With the threshold of 80%, each OTU has approximately 13.4 nonzero counts, similar to that in the skin microbiome data analysis, to ensure reliable estimates of  $\kappa_{jp}$ ,  $\beta_{jp}$  and  $\Sigma$ . We specified hyperparameters similar to those in § 3.2. The MCMC simulation was run over 30,000 iterations, with the first 15,000 iterations discarded as burn-in. It took 0.75 hours for every 5,000 iterations on a M1 Mac.

Posterior mean estimates  $\hat{\rho}_{jj'}$  of the marginal correlations (lower left triangle) are illustrated with naive empirical correlation estimates  $\rho_{jj'}^{em}$  (upper right triangle) in Fig 12(a). The figure shows relatively rich microbial interactions in the gut microbiome samples as reported in [Bashan \*et al.\* \(2016\)](#). Fig 12(b) reports  $\hat{\rho}_{jj'}$  for the OTUs having  $|\hat{\rho}_{jj'}| > 0.5$  for any  $j' \neq j$ , where the value of 0.5 is chosen to make the estimates in the figure readable. Taxonomic information of the OTUs in panel (b) is in Supp. Tab 6 ([Shuangjie \*et al.\*, 2022](#)). In panel (b), a group of OTUs 4, 31, 37, 39, 44, 56, 93 and 96 that are positively correlated with each other, are taxa that are found to indicate dysbiotic microbiota from gastrointestinal diseases. For example, OTUs 31 and 39 that belong to family *Erysipelotrichaceae* are observed to

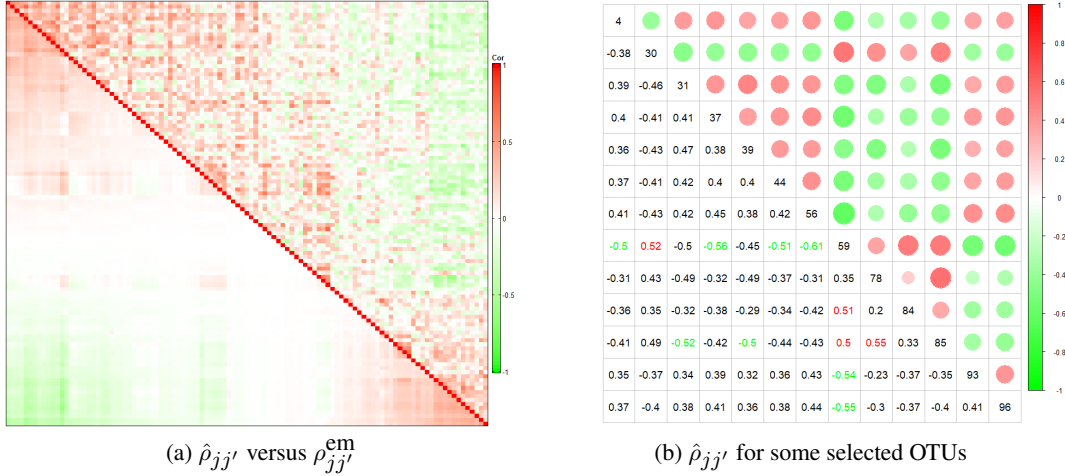


FIG 12. [Human Gut Microbiome Data]: Posterior marginal correlation estimates  $\hat{\rho}_{jj'}$  (lower left triangle) and empirical correlation estimates  $\rho_{jj'}^{em}$  (upper right triangle) are shown in panel (a). Panel (b) illustrates the OTUs having  $|\hat{\rho}_{jj'}| > 0.5$  for any  $j' \neq j$ .

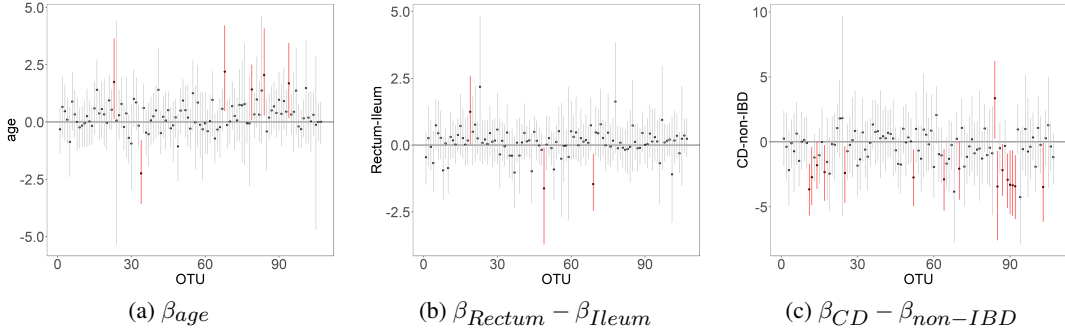


FIG 13. [Human Gut Microbiome Data] Posterior inference of regression coefficients  $\beta_{age}$ ,  $\beta_{Rectum} - \beta_{Ileum}$ , and  $\beta_{CD} - \beta_{non-IBD}$ , where the posterior mean estimates are denoted by dots, and the 95% credible estimates with vertical lines. The intervals that do not contain zero are marked.

be related to gastrointestinal inflammatory disorders (Kaakoush, 2015). And some species in *Escherichia* (OTU 93) (e.g., E. Coli (Mirsepasi-Lauridsen *et al.*, 2019)) and *Clostridium* (OTUs 31 and 96) (e.g., C. difficile (Nitzan *et al.*, 2013)) are known to be related to the development of IBD. Another group of OTUs that are positively associated with each other includes genera, *Bacteroides* (OTU 59), *Faecalibacterium* (OTU 30), *Lachnospiraceae* (OTU 84) and *Ruminococcaceae* (OTU 85). The group of those genera contains species that were found active in metabolic processes and can produce short-chain fatty acids (Parada Venegas *et al.*, 2019). These species might interact through exchanging metabolic products; for example, *Bacteroides thetaiotaomicron* and *Faecalibacterium prausnitzii* were found metabolically complementary, where the former is an acetate producer, and the latter is acetate consumer and butyrate producer (Wrzosek *et al.*, 2013). Furthermore, such metabolic functions might be part of a complex interplay between the microbiota and disease states. For example, butyrate is an anti-inflammation promoter, and the decrease of butyrate producers might also indicate dysbiotic gut microbiota (Andrade *et al.*, 2020). Interestingly, the OTUs in those two groups are negatively associated. The correlation patterns between the groups indicate how gut microbiota may shift from dysbiosis and may suggest further investigation through experiments. From taxonomic information in Supp. Tab 6 (Shuangjie *et al.*, 2022), the OTUs



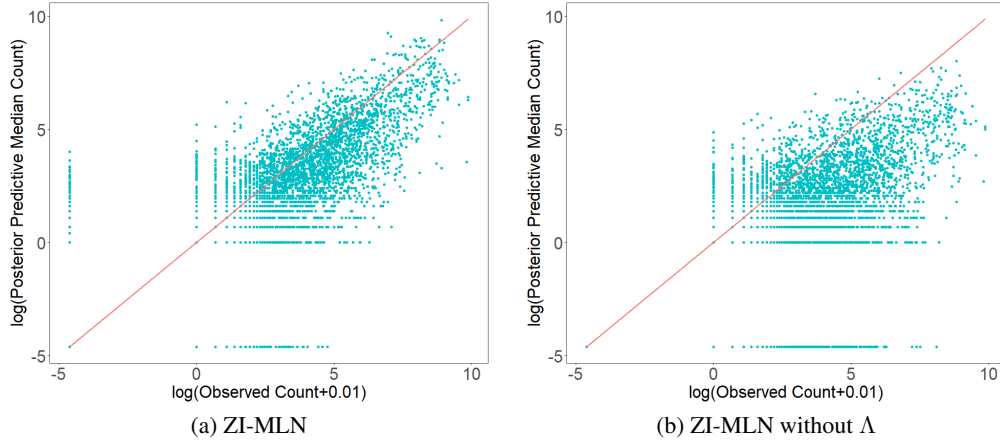


FIG 14. [Human Gut Microbiome Data: Comparison]: Panels (a) and (b) have scatter plots of observed  $\log(y_{ij} + 0.01)$  versus  $\log(\hat{y}_{ij}^{pred} + 0.01)$  under ZI-MLN and ZI-MLN without  $\Lambda$ , respectively.

in the groups belong to different families and orders, indicating that phylogenetically distant OTUs interact in gut microbiota.

Fig 13 and Supp. Fig 39(a)-(b) (Shuangjie *et al.*, 2022) illustrate posterior mean estimates  $\hat{\beta}_{jp}$  and  $\hat{\kappa}_{jp}$  of the regression coefficients, respectively, with their 95% credible intervals for some selected covariates. Dots represent point estimates and vertical lines interval estimates. In the figures,  $\beta_{jp}$  and  $\kappa_{jp}$  that do not contain zero in their 95% credible interval are marked. In addition, Supp. Tabs 7 and 8 (Shuangjie *et al.*, 2022) provide taxonomic information of the OTUs whose abundance or presence/absence is statistically associated with change in covariates. Overall, the covariate effects are statistically significant for a small number of OTUs. From panel (c), the effect of having condition CD compared to non-IBD  $\beta_{CD} - \beta_{non-IBD}$  is statistically significant for 16 OTUs. The effect estimates are negative for those except for OTU 84, which implies that their abundance is lower for a subject with CD than for a subject with non-IBD. Also, among those, 14 OTUs belong to phylum *Firmicutes* and order *Clostridiales*. Significant decrease in abundance of phylum *Firmicutes* (*Clostridium leptum* and *Clostridium coccoides* groups) in active IBD subjects compared to that in non-IBD subjects is reported in Sokol *et al.* (2009), Vester-Andersen *et al.* (2019) and Alam *et al.* (2020). Lloyd-Price *et al.* (2019) also reported a statistically significant decrease in abundance of *Clostridium leptum* in active IBD subjects. We compare posterior predictive median estimates of OTU counts to the observed data in Fig 14(a) to assess the model fit. The figure shows that the model fits the data well.

For comparison, we applied the comparators, SparCC, SPIEC-EASI, CCLasso and Zi-LN to the gut microbiome data. Fig 15 illustrates  $\hat{\rho}_{jj'}$  under the comparators. Also, additional comparators, ZI-MLN without  $\Lambda$ , metagenomeSeq and edgeR were applied. The first set of the comparators does not account for covariate effects, and the second set does not infer the dependence structure between OTUs. SPIEC-EASI yields a very sparse estimate, whereas the other comparators produce very dense estimates. Supp. Figs 39(c)-(d) and 40 (Shuangjie *et al.*, 2022) illustrate posterior estimates of regression coefficients  $\beta_{jp}$  and  $\kappa_{jp}$  obtained by the second set of the comparators. While ZI-MLN without  $\Lambda$  yields similar estimates, the estimates under metagenomeSeq and edgeR are greatly different from those under ZI-MLN. Specifically, under metagenomeSeq, the effects of covariate *age* are positive and statistically significant for most OTUs. A similar pattern is also observed from edgeR. For ZI-MLN without  $\Lambda$ , we further examine posterior predictive distributions of OTU counts (shown in



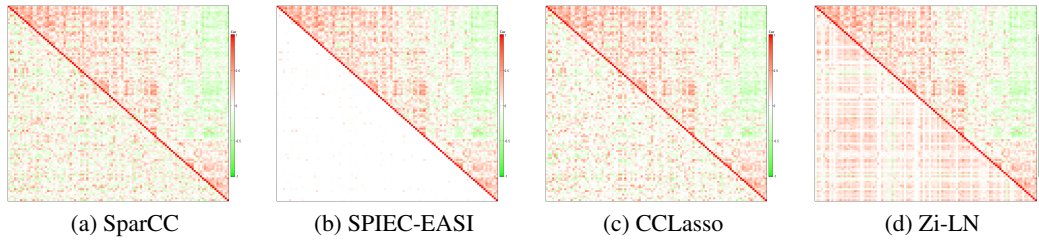


FIG 15. [Human Gut Microbiome Data: Comparison] Correlation estimates  $\hat{\rho}_{jj'}$  by SparCC, SPIEC-EASI, CCLasso and Zi-LN (lower left triangle) and empirical correlation estimates  $\rho_{jj'}^{em}$  (upper right triangle) are shown in panel (a)-(d), respectively.

Fig 14(b)). Compared to the fit under ZI-MLN, ZI-MLN without  $\Lambda$  yields a poor fit, especially for large counts. Supp. Fig 41 (Shuangjie *et al.*, 2022) compares mean abundance estimates under edgeR and metagenomeSeq to the observed counts and indicates poor model fit under those models.

**5. Discussion.** We have presented a Bayesian zero-inflated rounded log-normal kernel model to analyze multivariate count data with excess zeros. Different from most existing models, the model directly infers interrelationships between counts and produces reliable inference on microbial interaction with a small sample size. It offers a straightforward interpretation of microbial dependence structures. Furthermore, the model simultaneously incorporates covariates and accounts for excess zeros. The simulations showed that the developed model compares very favorably in parameter estimation and model fit to a model that ignores between-OTUs' dependence structure and some popular alternatives that do not model covariate effects and/or dependence structure.

ZI-MLN can be further extended to accommodate more complex data structures. Specifically, Lloyd-Price *et al.* (2019) collected multi-omics data to obtain a comprehensive understanding of the IBD microbial ecosystem. Multi-omic measurements from the same subject may be interrelated, and joint analysis of bacterial sequencing data with other types of sequencing data such as viral sequencing data can be useful. In general, latent factor models provide a convenient way to model complex interrelationship structures in multivariate data and can be extended to accommodate multiple coupled observation matrices, e.g., a group factor model (Zhao *et al.*, 2016). In that vein, our ZI-MLN can be extended to jointly analyze multiple correlated count matrices from a multi-omics study using an approach of a group factor model. Another possible extension is to incorporate phylogenetic information into the model. Investigating potential interactions between phylogenetically related microbes is biologically interesting, e.g., see Faust *et al.* (2012); Connor, Barberán and Clauset (2017); Kamneva (2017). Similar to Lo and Marculescu (2018), phylogenetic information can be utilized in building a prior model of  $\Sigma$ .

**Acknowledgements.** This work was supported by NIH: DP2 GM123457-01 to IAC (Irene Chen) and NSF grant DMS-1662427 (Juhee Lee).

## SUPPLEMENTARY MATERIAL

### Supplementary File **Supplementary material: Additional Results**

The Supplementary Material consists of four sections. In Supp. § 1, we provide details of the posterior computation. Supp. § 2 has additional results from the simulation studies. Supp. § 3 contains additional results of the real data analyses.

**Supplementary material: ZI-MLN Code**

The supplementary source code contains the implementation of the models described in the paper. It is also available from <https://github.com/Zsj950708/ZI-MLN>.

## REFERENCES

- AGARWAL, D. K., GELFAND, A. E. and CITRON-POUSTY, S. (2002). Zero-inflated models with application to spatial count data. *Environmental and Ecological statistics* **9** 341–355.
- ALAM, M. T., AMOS, G. C., MURPHY, A. R., MURCH, S., WELLINGTON, E. M. and ARASARADNAM, R. P. (2020). Microbial imbalance in inflammatory bowel disease patients at different taxonomic levels. *Gut pathogens* **12** 1–8.
- ANDRADE, J. C., ALMEIDA, D., DOMINGOS, M., SEABRA, C. L., MACHADO, D., FREITAS, A. C. and GOMES, A. M. (2020). Commensal obligate anaerobic bacteria and health: production, storage, and delivery strategies. *Frontiers in Bioengineering and Biotechnology* **8** 550.
- BASHAN, A., GIBSON, T. E., FRIEDMAN, J., CAREY, V. J., WEISS, S. T., HOHMANN, E. L. and LIU, Y.-Y. (2016). Universality of human microbial dynamics. *Nature* **534** 259–262.
- BHATTACHARYA, A. and DUNSON, D. B. (2011). Sparse Bayesian infinite factor models. *Biometrika* 291–306.
- BHATTACHARYA, A., PATI, D., PILLAI, N. S. and DUNSON, D. B. (2015). Dirichlet–Laplace priors for optimal shrinkage. *Journal of the American Statistical Association* **110** 1479–1490.
- BIEN, J. and TIBSHIRANI, R. J. (2011). Sparse estimation of a covariance matrix. *Biometrika* **98** 807–820.
- CAI, T., LIU, W. and LUO, X. (2011). A constrained L1 minimization approach to sparse precision matrix estimation. *Journal of the American Statistical Association* **106** 594–607.
- CAI, T., MA, Z. and WU, Y. (2015). Optimal estimation and rank detection for sparse spiked covariance matrices. *Probability theory and related fields* **161** 781–815.
- CAI, T. T., REN, Z. and ZHOU, H. H. (2016). Estimating structured high-dimensional covariance and precision matrices: Optimal rates and adaptive estimation. *Electronic Journal of Statistics* **10** 1–59.
- CAI, Z., ZHU, T., LIU, F., ZHUANG, Z. and ZHAO, L. (2021). Co-pathogens in Periodontitis and Inflammatory Bowel Disease. *Frontiers in Medicine* **8**.
- CANALE, A. and DUNSON, D. B. (2011). Bayesian kernel mixtures for counts. *Journal of the American Statistical Association* **106** 1528–1539.
- CHATTOPADHYAY, S., ARNOLD, J. D., MALAYIL, L., HITTLE, L., MONGODIN, E. F., MARATHE, K. S., GOMEZ-LOBO, V. and SAPKOTA, A. R. (2021). Potential role of the skin and gut microbiota in premenarchal vulvar lichen sclerosis: A pilot case-control study. *PLoS one* **16** e0245243.
- CONNOR, N., BARBERÁN, A. and CLAUSET, A. (2017). Using null models to infer microbial co-occurrence networks. *PLoS one* **12** e0176751.
- FANG, H., HUANG, C., ZHAO, H. and DENG, M. (2015). CCLasso: correlation inference for compositional data through Lasso. *Bioinformatics* **31** 3172–3180.
- FAUST, K., SATHIRAPONGSASUTI, J. F., IZARD, J., SEGATA, N., GEVERS, D., RAES, J. and HUTTENHOWER, C. (2012). Microbial co-occurrence relationships in the human microbiome. *PLoS computational biology* **8** e1002606.
- FRIEDMAN, J. and ALM, E. J. (2012). Inferring correlation networks from genomic survey data.
- FRIEDMAN, J., HASTIE, T. and TIBSHIRANI, R. (2008). Sparse inverse covariance estimation with the graphical lasso. *Biostatistics* **9** 432–441.
- GAO, C. and ZHOU, H. H. (2015). Rate-optimal posterior contraction for sparse PCA. *The Annals of Statistics* **43** 785–818.
- GRANTHAM, N. S., GUAN, Y., REICH, B. J., BORER, E. T. and GROSS, K. (2020). Mimix: A bayesian mixed-effects model for microbiome data from designed experiments. *Journal of the American Statistical Association* **115** 599–609.
- JIANG, S., XIAO, G., KOH, A. Y., KIM, J., LI, Q. and ZHAN, X. (2021). A Bayesian zero-inflated negative binomial regression model for the integrative analysis of microbiome data. *Biostatistics* **22** 522–540.
- JOVEL, J., PATTERSON, J., WANG, W., HOTTE, N., O’KEEFE, S., MITCHEL, T., PERRY, T., KAO, D., MASON, A. L., MADSEN, K. L. et al. (2016). Characterization of the gut microbiome using 16S or shotgun metagenomics. *Frontiers in microbiology* **7** 459.
- KAAKOUSH, N. O. (2015). Insights into the Role of Erysipelotrichaceae in the Human Host. *Frontiers in Cellular and Infection Microbiology* **5** 84.
- KAMNEVA, O. K. (2017). Genome composition and phylogeny of microbes predict their co-occurrence in the environment. *PLoS computational biology* **13** e1005366.
- KURTZ, Z. D., MÜLLER, C. L., MIRALDI, E. R., LITTMAN, D. R., BLASER, M. J. and BONNEAU, R. A. (2015). Sparse and compositionally robust inference of microbial ecological networks. *PLoS computational biology* **11** e1004226.

- LEE, J. and SISON-MANGUS, M. (2018). A Bayesian semiparametric regression model for joint analysis of microbiome data. *Frontiers in microbiology* **9** 522.
- LI, Q., GUINDANI, M., REICH, B. J., BONDELL, H. D. and VANNUCCI, M. (2017). A Bayesian mixture model for clustering and selection of feature occurrence rates under mean constraints. *Statistical Analysis and Data Mining: The ASA Data Science Journal* **10** 393–409.
- LLOYD-PRICE, J., ARZE, C., ANANTHAKRISHNAN, A. N., SCHIRMER, M., AVILA-PACHECO, J., POON, T. W., ANDREWS, E., AJAMI, N. J., BONHAM, K. S., BRISLAWN, C. J. et al. (2019). Multi-omics of the gut microbial ecosystem in inflammatory bowel diseases. *Nature* **569** 655–662.
- LO, C. and MARCULESCU, R. (2018). PGLasso: Microbial Community Detection through Phylogenetic Graphical Lasso. <https://arxiv.org/abs/1807.08039v1>.
- MA, S., REN, B., MALLICK, H., MOON, Y. S., SCHWAGER, E., MAHARJAN, S., TICKLE, T. L., LU, Y., CARMODY, R. N., FRANZOSA, E. A. et al. (2021). A statistical model for describing and simulating microbial community profiles. *PLoS computational biology* **17** e1008913.
- MAO, J., CHEN, Y. and MA, L. (2020). Bayesian graphical compositional regression for microbiome data. *Journal of the American Statistical Association* **115** 610–624.
- MIRSEPASI-LAURIDSEN, H. C., VALLANCE, B. A., KROGFELT, K. A. and PETERSEN, A. M. (2019). Escherichia coli pathobionts associated with inflammatory bowel disease. *Clinical microbiology reviews* **32** e00060–18.
- NITZAN, O., ELIAS, M., CHAZAN, B., RAZ, R. and SALIBA, W. (2013). Clostridium difficile and inflammatory bowel disease: role in pathogenesis and implications in treatment. *World journal of gastroenterology: WJG* **19** 7577.
- PARADA VENEGAS, D., DE LA FUENTE, M. K., LANDSKRON, G., GONZÁLEZ, M. J., QUERA, R., DIJKSTRA, G., HARMSSEN, H. J., FABER, K. N. and HERMOSO, M. A. (2019). Short chain fatty acids (SCFAs)-mediated gut epithelial and immune regulation and its relevance for inflammatory bowel diseases. *Frontiers in immunology* **277**.
- PARK, J.-U., OH, B., LEE, J. P., CHOI, M.-H., LEE, M.-J. and KIM, B.-S. (2019). Influence of microbiota on diabetic foot wound in comparison with adjacent normal skin based on the clinical features. *BioMed research international* **2019**.
- PATI, D., BHATTACHARYA, A., PILLAI, N. S., DUNSON, D. et al. (2014). Posterior contraction in sparse Bayesian factor models for massive covariance matrices. *Annals of Statistics* **42** 1102–1130.
- PAULSON, J. N., STINE, O. C., BRAVO, H. C. and POP, M. (2013). Differential abundance analysis for microbial marker-gene surveys. *Nature methods* **10** 1200–1202.
- PROST, V., GAZUT, S. and BRÜLS, T. (2021). A zero inflated log-normal model for inference of sparse microbial association networks. *PLoS Computational Biology* **17** e1009089.
- QIN, J., SHI, X., XU, J., YUAN, S., ZHENG, B., ZHANG, E., HUANG, G., LI, G., JIANG, G., GAO, S. et al. (2021). Characterization of the genitourinary microbiome of 1,165 middle-aged and elderly healthy individuals. *Frontiers in Microbiology* **12**.
- REN, B., BACALLADO, S., FAVARO, S., VATANEN, T., HUTTENHOWER, C. and TRIPPA, L. (2017). Bayesian nonparametric mixed effects models in microbiome data analysis. *arXiv preprint arXiv:1711.01241*.
- ROBINSON, M. D., MCCARTHY, D. J. and SMYTH, G. K. (2010). edgeR: a Bioconductor package for differential expression analysis of digital gene expression data. *Bioinformatics* **26** 139–140.
- SCHWAGER, E., MALLICK, H., VENTZ, S. and HUTTENHOWER, C. (2017). A Bayesian method for detecting pairwise associations in compositional data. *PLoS computational biology* **13** e1005852.
- SHUANGJIE, Z., YUNING, S., IRENE A., C. and JUHEE, L. (2022). Supplement to "Bayesian Modeling of Interaction between Features in Sparse Multivariate Count Data with Application to Microbiome Study".
- SHULER, K., VERBANIC, S., CHEN, I. A. and LEE, J. (2021). A Bayesian nonparametric analysis for zero-inflated multivariate count data with application to microbiome study. *Journal of the Royal Statistical Society: Series C (Applied Statistics)*.
- SOKOL, H., SEKSIK, P., FURET, J., FIRMESSE, O., NION-LARMURIER, I., BEAUGERIE, L., COSNES, J., CORTHIER, G., MARTEAU, P. and DORÉ, J. (2009). Low counts of Faecalibacterium prausnitzii in colitis microbiota. *Inflammatory bowel diseases* **15** 1183–1189.
- TANG, Z.-Z. and CHEN, G. (2019). Zero-inflated generalized Dirichlet multinomial regression model for microbiome compositional data analysis. *Biostatistics* **20** 698–713.
- VERBANIC, S., SHEN, Y., LEE, J., DEACON, J. M. and CHEN, I. A. (2020). Microbial predictors of healing and short-term effect of debridement on the microbiome of chronic wounds. *NPJ biofilms and microbiomes* **6** 1–11.
- VESTER-ANDERSEN, M., MIRSEPASI-LAURIDSEN, H., PROSBERG, M., MORTENSEN, C., TRÄGER, C., SKOVSEN, K., THORKILGAARD, T., NØJGAARD, C., VIND, I., KROGFELT, K. A. et al. (2019). Increased abundance of proteobacteria in aggressive Crohn's disease seven years after diagnosis. *Scientific reports* **9** 1–10.

- WADSWORTH, W. D., ARGIENTO, R., GUINDANI, M., GALLOWAY-PENA, J., SHELBURNE, S. A. and VANNUCCI, M. (2017). An integrative Bayesian Dirichlet-multinomial regression model for the analysis of taxonomic abundances in microbiome data. *BMC bioinformatics* **18** 1–12.
- WANG, Z., MAO, J. and MA, L. (2021). Logistic-tree normal model for microbiome compositions. *arXiv preprint arXiv:2106.15051*.
- WANG, T. and ZHAO, H. (2017). A Dirichlet-tree multinomial regression model for associating dietary nutrients with gut microorganisms. *Biometrics* **73** 792–801.
- WRZOSEK, L., MIQUEL, S., NOORDINE, M.-L., BOUET, S., CHEVALIER-CURT, M. J., ROBERT, V., PHILIPPE, C., BRIDONNEAU, C., CHERBUY, C., ROBBE-MASSELOT, C. et al. (2013). *Bacteroides thetaio-*taomicron and *Faecalibacterium prausnitzii* influence the production of mucus glycans and the development of goblet cells in the colonic epithelium of a gnotobiotic model rodent. *BMC biology* **11** 1–13.
- XIA, F., CHEN, J., FUNG, W. K. and LI, H. (2013). A logistic normal multinomial regression model for microbiome compositional data analysis. *Biometrics* **69** 1053–1063.
- XIAOMING, W., JING, L., YUCHEN, P., HUILI, L., MIAO, Z. and JING, S. (2021). Characteristics of the vaginal microbiomes in prepubertal girls with and without vulvovaginitis. *European Journal of Clinical Microbiology & Infectious Diseases* **40** 1253–1261.
- XIE, F., XU, Y., PRIEBE, C. E. and CAPE, J. (2018). Bayesian estimation of sparse spiked covariance matrices in high dimensions. *arXiv preprint arXiv:1808.07433*.
- ZHANG, X., MALLICK, H., TANG, Z., ZHANG, L., CUI, X., BENSON, A. K. and YI, N. (2017). Negative binomial mixed models for analyzing microbiome count data. *BMC bioinformatics* **18** 1–10.
- ZHAO, S., GAO, C., MUKHERJEE, S. and ENGELHARDT, B. E. (2016). Bayesian group factor analysis with structured sparsity. *The Journal of Machine Learning Research* **17** 6868–6914.